Periodic multichannel Thomson scattering in ASDEX

H. Röhr, K.-H. Steuer, H. Murmann, D. Meisel

IPP III/121 B

Juli 1987

MAX-PLANCK-INSTITUT FÜR PLASMAPHYSIK

8046 GARCHING BEI MÜNCHEN

MAX-PLANCK-INSTITUT FÜR PLASMAPHYSIK

GARCHING BEI MÜNCHEN

Periodic multichannel Thomson scattering in ASDEX

H. Röhr, K.-H. Steuer, H. Murmann, D. Meisel

IPP III/121 B Juli 1987

Die nachstehende Arbeit wurde im Rahmen des Vertrages zwischen dem Max-Planck-Institut für Plasmaphysik und der Europäischen Atomgemeinschaft über die Zusammenarbeit auf dem Gebiete der Plasmaphysik durchgeführt.

Concerning: IPP-Report IPP III/121 B
Periodic Multichannel....

Erratum: The correct version of formula (24), page 38, is:

$$\rho(z,t) = \frac{a}{\Delta_0(t)\sqrt{2}} \sqrt{A(t) - \sqrt{A(t)^2 - 4\,\Delta_0{}^2(t) \cdot [D^2(t) + z_1{}^2(t)]}} \qquad (24)$$

IPP III/121 H.Röhr
K.-H.Steuer
H.Murmann
D.Meisel

Periodic multichannel
Thomson scattering in ASDEX

ABSTRACT.

The optical and electronic design of the Thomson scattering experiment in the ASDEX-Tokamak is described. This Thomson scattering system is employed as a standard diagnostic for the evaluation of electron temperature and density simultaneously at 16 spatial points in ASDEX. The light source is a Nd-YAG laser emitting at 1.06 μm wavelength, which is capable of delivering 60 pulses per second for a period of about 7 sec. This period includes the whole ASDEX plasma discharge. The scattered light is detected by Si-avalanche diodes. Density calibration is carried out by rotational anti-Stokes Raman scattering from molecular hydrogen. The system is capable of measuring densities as low as $5 \times 10^{12}\, cm^{-3}$ and electron temperatures in the range from 150 eV to 5 keV. The data-processing system and the calculations which lead to the final output of Te/Ne-profiles are discussed. Examples of profile measurements are given showing the possibilities of the system under various plasma conditions.

Technical details of the system are described in tables listed in the appendix.

CONTENTS.

Periodic Multichannel Thomson Scattering in ASDEX

H. Röhr, K.-H. Steuer, H. Murmann, D. Meisel

PREFACE.

This laboratory report describes a Thomson scattering experiment with a multi-pulse laser in the ASDEX tokamak experiment. To help the reader not specialized in scattering to follow this report, it is divided into three sections:

The first section summarizes the experiment. The second section gives a detailed account of the individual components and the procedures. In the third section (appendix), the most important details of the experiment are collected in tabular form.

It is taken for granted that the physical principles of laser scattering are known, and so they are only briefly treated.

1. Overview

Although Thomson scattering has been used to measure electron temperature (Te) and electron density (Ne) in plasmas since 1963 [**1**], it was not till 1969 that scattering measurements were first made in a tokamak, by a British group in Moscow on the T3 experiment [**2**]. The difficulty in comparison with previous scattering experiments in pinches lay primarily in the comparatively low electron density of tokamaks and the relatively low output powers of standard lasers at the time. This measurement demonstrated experimentally without a doubt that the presumed electron temperature of 10 million degrees had, in fact, been attained in T3.

All scattering measurements and this first one in a tokamak impressively demonstrated two great advantages of the method in Te/Ne measurements:

- determination of the electron temperature requires only the assumption of a Maxwellian electron velocity distribution;

- spatially resolved measurement of Te/Ne is possible.

For both the scattering experiment in the T3 plasma and all subsequent scattering experiments (e.g. Pulsator, ST, ASDEX), however, it was quite troublesome to conduct plasma parameter studies because for each plasma discharge the scattering apparatus only yielded temperature and density values at a single time. Measurement of the time development of Te/Ne called for large series of reproducible discharges, which were difficult to achieve.

Efforts were therefore begun to increase the number of measurements per plasma discharge:

1) by increasing the number of experimental points along the laser beam in the plasma,
2) by means of multi-pulse ruby lasers [**3**].

Point 1 was realized in the new, larger tokamaks with improved accessibility (ASDEX, PLT, etc.). With the ruby laser scattering system in ASDEX, for example, it was possible in each plasma discharge to measure a Te- and Ne-profile composed of ten spatial points; a separate system provides five points in the plasma edge [**4**]. The achievement of point 2 was severely limited by the poor thermal conductivity of the ruby laser rods.

The objective of the Thomson scattering experiment with multiple laser pulses was, from the outset, to measure electron temperature and density profiles during the entire discharge time in the ASDEX tokamak experiment. The development of the system was started about 10 years ago as a joint project with Institut für Plasmaforschung (IPF) of the University of Stuttgart.

First a periodically operating scattering system with just one spatial channel and 400 pulses at 60 Hz rate was constructed and successfully operated in ASDEX at IPP [**5**]. This was followed by the design and construction of an enlarged system composed of 16 spatial channels and likewise operated at 60 Hertz. This new system has now been working as one of the standard diagnostics in ASDEX for 1 1/2 years to the complete satisfaction of the ASDEX team. Measurement is almost automatic; the data are available to every user

shortly after each plasma discharge.

The main advantage of the multi-pulse Thomson scattering compared with conventional scattering apparatus is that the entire discharge lasting several seconds can be diagnosed. In addition, the new system has a few further advantages over previously available ruby laser scattering systems:

- the Nd-YAG laser used emits at 1.06 μm. The plasma light at this wavelength is much less intense than at 0.7 μm (ruby).
- The detectors required at 1 μm (Si-avalanche-diodes) have a much higher quantum efficiency than photomultipliers. It is between 40 and 80% in the wavelength range from 0.7 to 1.0 μm.
- The diodes are linear over a wider intensity range than photomultipliers.
- The diodes are insensitive to the magnetic field.
- The Nd-YAG laser has proved to be very reliable in practice, and so maintenance and repair work has been almost negligible.

1.1 The Characteristics of multi-pulse Thomson Scattering in ASDEX.

In the following the essential characteristics of the scattering experiment are summarized. A description in more detail is given in the following chapters.

The layout is basically the same as that of a standard 90° scattering experiment (see Fig. 1). The laser penetrates the plasma vertically from bottom to top. A specially corrected lens images the scattering plasma on to the entrance slits of 16 polychromators. The plasma domain observed extends from the bottom plasma edge (– 40 cm) to half the upper plasma radius (+ 20 cm). A small amount of laser light is picked off at the beam exit and is used for triggering and for calibration and control purposes as well.

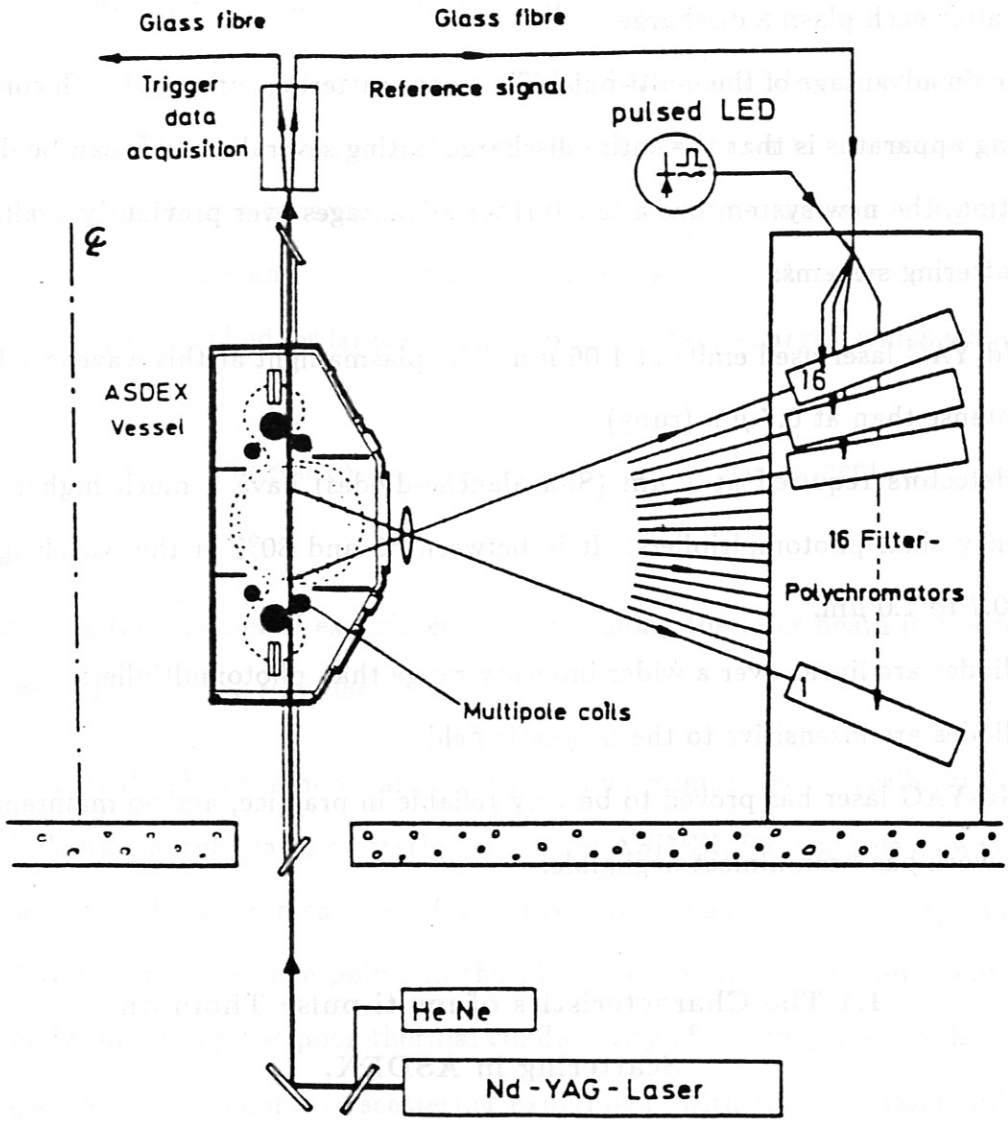

Fig.1: Optical layout for Thomson scattering in ASDEX.

In each polychromator the spectral dispersion is performed by three interference filters. They have particularly steep wings in order to suppress the stray light at the laser wavelength as much as possible. The short-wavelength side of the scattering spectrum is divided into three domains which are roughly matched to the temperatures expected. The scattered light is detected with Si-avalanche-photodiodes.

The signals of the diodes are automatically recorded by the ASDEX data acquisition system and processed after the discharge. The electron temperature is calculated from the ratio of the scattering signals of two spectral channels [6]. The density is determined by using the absolute intensity of one spectral channel (Raman calibration) and the calculated temperature. After a calculation time of a few seconds, one has for every point in space and time a pair of values $T_e(z,t)$, $Ne(z,t)$, which can be represented as required in two or three-dimensional plots or are transferred to sucessive evaluation programmes.

The spectral arrangement of the measuring channels and the statistical fluctuations of the measuring signals govern the experimental limits of the system:

Electron temperature:

150 eV	$\leq Te \leq$	5000 eV	
boundary		centre	

Electron density:

$$N_e \geq 5 \times 10^{12}\ cm^{-3}$$

By averaging in time over a larger number of laser pulses it is possible to shift the stated density limit to lower densities at the expense of time resolution.

1.2 Examples of the Measurements.

The following figures present examples of ASDEX measurements in various formats:

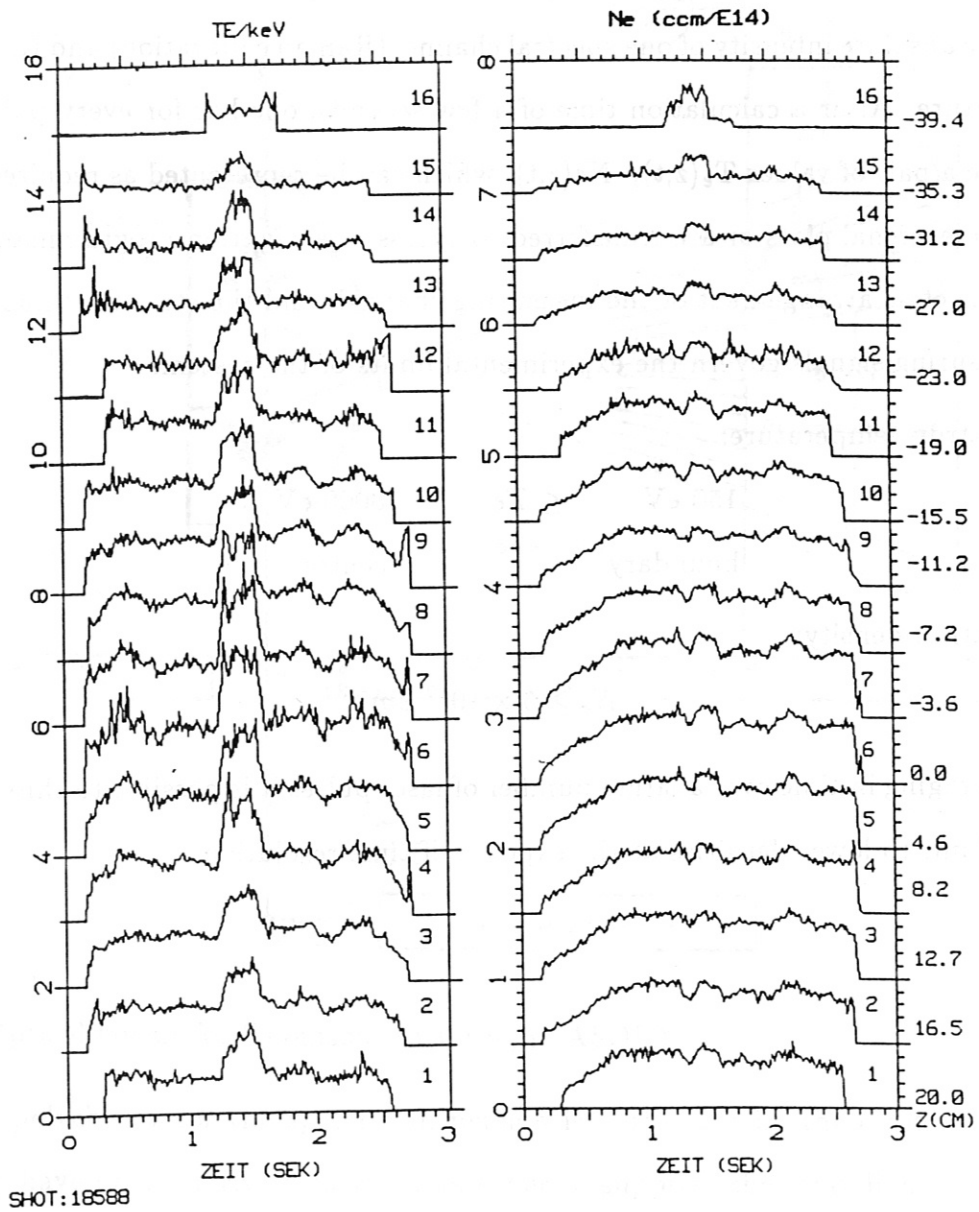

Fig.2: Typical plot of Te and Ne values as a function of time. The plasma discharge begins at the time t=0 s. Te and Ne values are only specified when the scattering signals exceed a certain threshold, which is mainly governed by the density and noise. The Te and Ne values in the plot therefore are set zero till times t≈0.1 s. Neutral injection was applied from 1.2 to 1.5 s.

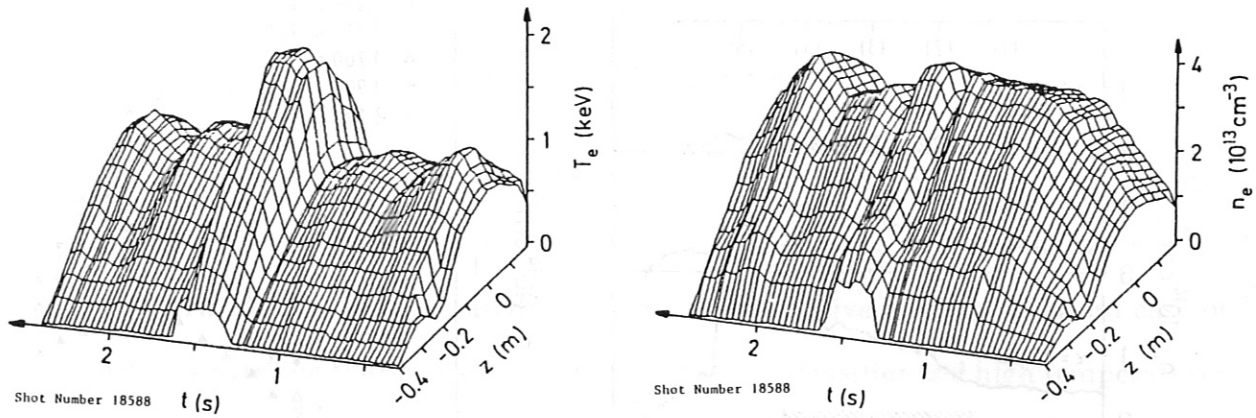

Fig.3: Example of a three-dimensional plot of Te(z,t) and Ne(z,t) during a discharge with neutral injection as additional heating (P_{NI} = 3 MW). Only alternate profiles are plotted. The variation of the profiles, particularly at the plasma boundary, during neutral injection (1.2 – 1.6 s) shows that the discharge has entered the regime with good confinement (H-regime).

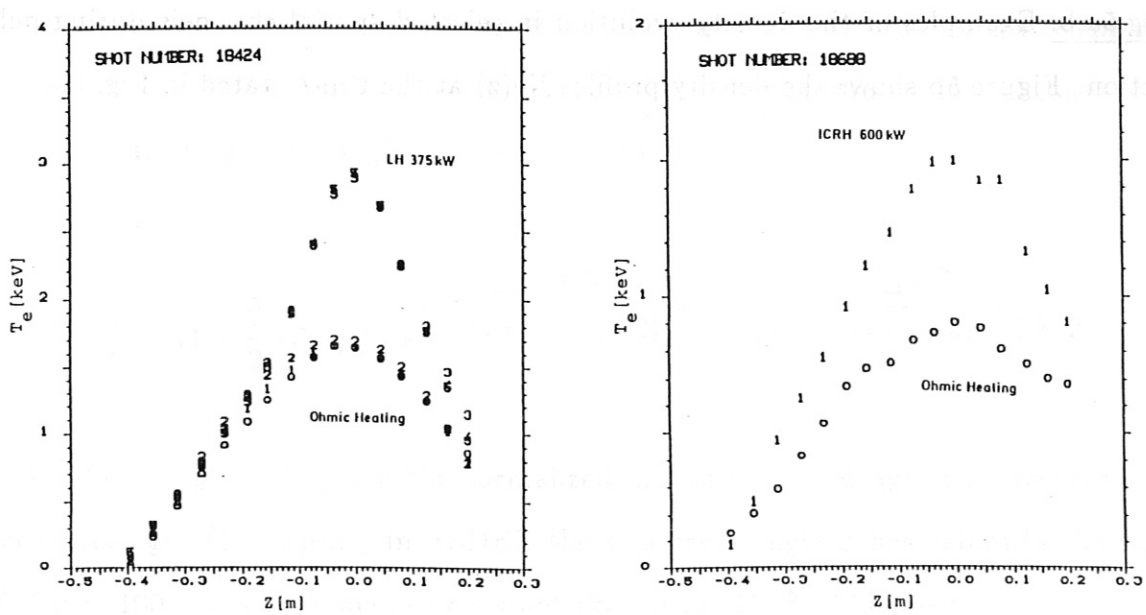

Fig.4: Plots of profile variation of Te(z) during various heating methods in ASDEX. The open circles show Te-profiles in the ohmic part of plasma discharge just before the additional heating is switched on. With the Lower Hybrid heating (LH) the profiles were measured at densities of about $6 \times 10^{12} cm^{-3}$, while with the Ion Cyclotron Resonance Heating (ICRH) the densities were about $3 \times 10^{13} cm^{-3}$.

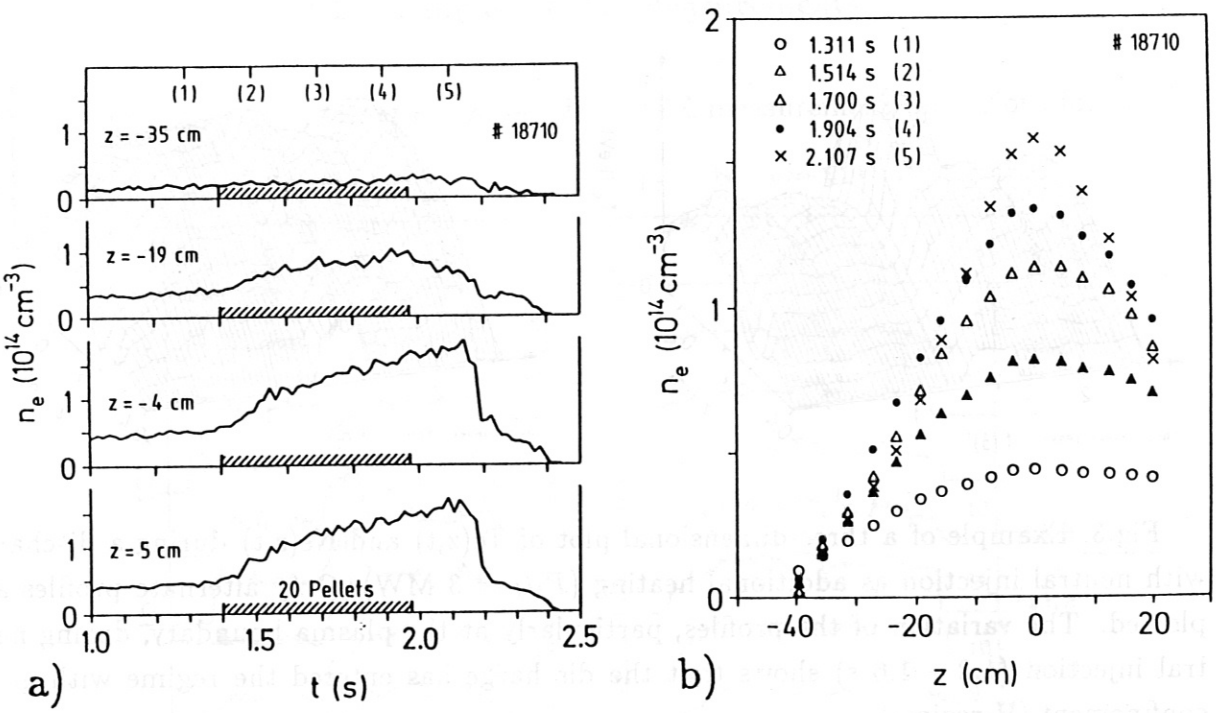

Fig.5a,b: Examples of the density evolution in selected spatial channels during pellet injection. Figure 5b shows the density profiles Ne(z) at the times stated in Fig. 5a.

2. Detailed Description of the Scattering Experiment.

2.1 Physical Principles.

It is taken for granted that the physical principles of laser scattering are known. Appropriate information is given, for example, in the basic studies of Salpeter [7] and Kunze [8].

With scattering in the near infrared, it is always the relatively straightforward case of non-collective scattering that is involved, owing to the low densities and high temperatures in tokamaks. The scattering spectrum is then almost a direct mapping of the electron velocity distribution projected in the direction of the scattering vector. This means that in the case of a Maxwellian electron velocity distribution the scattering spectrum is represented by a bell-shaped curve, the half-width of which yields the temperature, and the total magnitude of which yields the density.

At temperatures above 500 eV deviations in the gaussian shape of the scattering spectrum occur (socalled relativistic effects). These deviations are taken into account in the following scattering formula given by Sheffield [9] :

$$I(\lambda) \sim (1 - \frac{7}{2}(\Delta\lambda)) * e^{-\frac{63868\,eV}{kT_e * sin^2(\varphi/2)} * \frac{(\Delta\lambda)^2}{1 + \Delta\lambda + (sin(\varphi/2) * \Delta\lambda/2)^2}} \quad (1)$$

$\Delta\lambda = (\lambda - \lambda_{Laser})/\lambda_{Laser}$ is the normalized shift of the wavelength with respect to the laser wavelength (1.064 μm). In ASDEX the scattering angle φ has values in the region $75^0 \leq \varphi \leq 100^0$. k is Boltzmann's constant (k= $8.614 \cdot 10^{-5}$ eV/degree).

2.2 The design of the scattering apparatus.

2.21 The optical system.

Fig.1 already showed the layout of the scattering experiment at ASDEX. The mechanical structure in the inner part of the ASDEX vacuum vessel allows the laser beam to traverse ASDEX in vertical direction only through 2 cm wide slits between the multipoles. The scattered light is collected between angles of 75^0 and 100^0 by high f-number optics.

For geometric reasons, the measurement of temperature and density profiles in ASDEX is possible from the lower plasma edge (–40 cm) up to +20 cm above the plasma center. The scattered light is spectrally analyzed in 16 polychromators equipped with 3 interference filters each. Thus the distance between channels is 4 cm. As the intensity of the scattered light increases with increasing length of the scattering volume, a scattering volume of maximum length should be imaged. The length we can use is restricted to 2.8 cm by the size of the polychromators.

The detection of the scattered light is done by Si-avalanche-diodes (3 per polychromator). The sensitive area of the avalanche diodes and the maximum f–number of the focussing optics limit the 'Etendue' of the path of the scattered light. This leads to an imaging lens with 23 cm diameter at a distance of 126 cm from the plasma center. The solid angle of the beam is therefore 2.6×10^{-2} sterad.

An evaluation of the signal-to-noise ratio[1] at the wavelength of a Nd-YAG laser ($1.064 \mu m$) with the assumption of a level of plasma light which is 100× Hydrogen Bremsstrahlung and with a laser energy of 1 J/pulse leads to a signal-to-noise of 10:1. A Nd-YAG laser with this pulse energy and a repetition frequency of about 100 Hz was not available. It had to be developed for our purposes.

[1] Estimations for other combinations of lasers and detectors are found in laboratory report [10]

2.22 The Nd-YAG laser.

The Nd-YAG laser was developed by the British laser company JK-Lasers in Rugby. In order to achieve reliable laser performance during the ASDEX experiments, the laser was built with approved standard elements. The resulting laser has proved reliability throughout several years at ASDEX.

In the following the essential components of the laser are briefly described[1]:

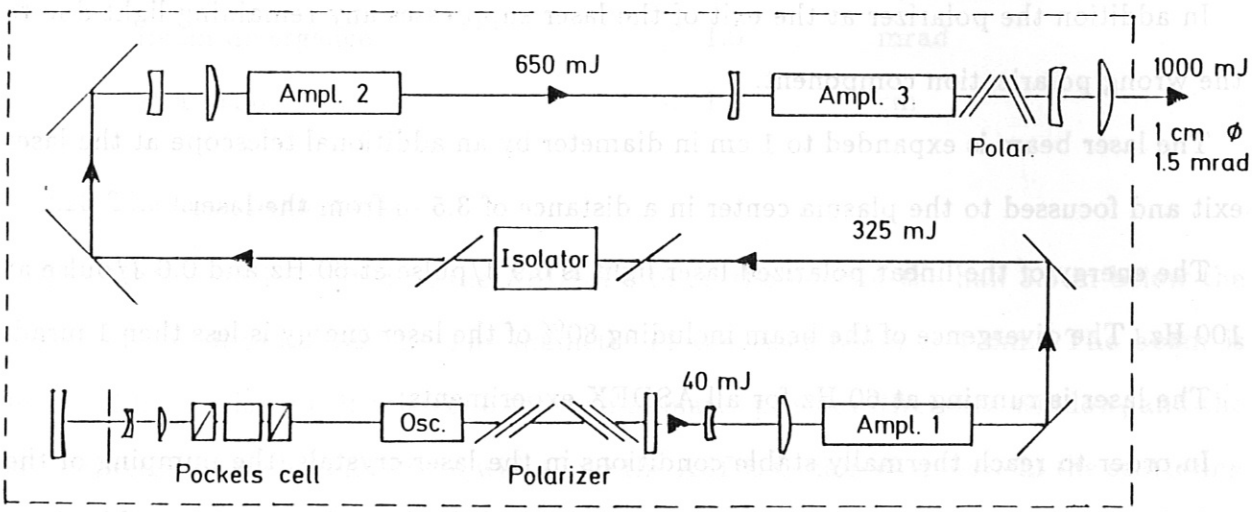

Fig.6: Schematic diagram of the Nd-YAG-Laser.

The laser is composed of one oscillator and three amplifiers. The oscillator ($4'' \times$ 4 mm diameter) is Q-switched by a Pockels cell (KD*P) and two Glan-polarizers. It works with a beamstop for selection of the single transverse mode. This selection is necessary in order to avoid destruction of the following laser rods by interference of different modes. The three amplifier rods have the same size $3'' \times 1/4''$.

Each laser rod is pumped by two flashlamps, which can be operated with repetition frequencies up to 100 Hz. The flashlamps are cooled by a nitrite-solution which absorbs the UV-radiation. The laser rods are cooled by distilled water. The inhomogenous distribution of temperature in the rods causes some lensing effect. This is compensated by external

[1] A detailed reference book for this type of laser (system 2800) is delivered with the laser by JK-Lasers

telescopes. The distances between the lenses of the telescopes must be adjusted with the repetition frequency of the laser. Every change of the repetition frequency of the laser therefore leads to a realignment of the laser optics. An optical isolator between amplifier 1 and 2 (KD*P-pockelscell + polarizer) prevents amplifiers from lasing.

The polarizer within the oscillator in conjunction with the optical isolator suppress the radiation with the polarization direction which is not necessary for the Thomson scattering and which may be destructive for the amplifiers.

In addition the polarizer at the exit of the laser suppresses any remaining light due to the wrong polarization component.

The laser beam is expanded to 1 cm in diameter by an additional telescope at the laser exit and focussed to the plasma center in a distance of 3.5 m from the laser.

The energy of the linear polarized laser light is 0.9 J/pulse at 60 Hz and 0.6 J/pulse at 100 Hz. The divergence of the beam including 80% of the laser energy is less then 1 mrad.

The laser is running at 60 Hz for all ASDEX experiments.

In order to reach thermally stable conditions in the laser crystals, the pumping of the rods by the flashlamps starts 3 s before the onset of the laser burst. After this time, the Pockels cell is switched periodically and the laser starts its operation. The maximum number of laser pulses is limited to 400 for thermal reasons.

The main technical parameters of the laser are summarized in the following table:

Wavelength		1.064	μm
Pulse frequency		60 (100)	1/sec
Duration of the pulse train	$\leq$	6.6 (4)	sec
Number of pulses		400	
Pulse-energy (linear pol.)	$\approx$	0.9 (0.6)	Ws
Pulse duration	$\approx$	30	ns
Beam divergence	$\leq$	1.0	mrad
at a beam diameter	$\approx$	1	cm

2.23 The laser beam path.

The YAG-laser is located at the ASDEX site on the floor of the hall 3.5 m below the center of the vacuum vessel. The diameter of the laser beam is 1 cm. The beam is focussed by the laser exit telescope through a quartz prism, a Brewster window, and the slit between the multipoles (2 cm wide) into the ASDEX main chamber. In the scattering region, which is 60 cm long, a beam diameter smaller then 2 mm is attained. The beam passes the geometrical center of the vacuum vessel at a distance of 1.75 cm towards the inside. The laser beam leaves the vessel through the upper multipole slit (2 cm wide) and a second Brewster window. The beam energy is now absorbed by a 10 cm thick package of greenish glass plates set at the Brewster angle. The absorbtion coefficient of the plates is relatively small, thus damage of the glass is prevented. A glass scatter-plate distributes the remaining light ($\approx$1%) on two lightguides:

1. One lightguide, which is as short as possible (9 m length), transmits light pulses to trigger the gates of the Analog-Digital-Converters (ADC's) of the datamation system;

2. A second lightguide (40 m long), transmits delayed reference light pulses to all 48 avalanche diodes.

The beam of a He-Ne-laser can be made colinear with the YAG-laser beam for purposes of alignment.

2.24 The Observation Beam Path

The scattered light emerging from the ASDEX vessel is imaged with a 4-lens-objective on the polychromators 4.4 m away.

The objective is located directly outside the vacuum window of the ASDEX vessel at a distance of 1.26 m from the centre of the vessel. Its diameter is 23 cm and its focal length 90 cm. It images a 60 cm long section of the scattering plasma magnified 2.5 times on the entrance slits (each 70 mm high and 10 mm wide) of the polychromators. The 4-lens-objective was specially corrected for these particular imaging conditions, attention being paid to keeping the curvature of the image plane small.

As a result of stacking the 16 polychromators 16 scattering volumes each 28 mm long and spaced 40 mm can be observed along the laser beam.

The window in the ASDEX vacuum vessel (40 cm in diameter) used for observation of the scattered light is made of 4 cm thick quartz. It can be protected on the plasma side with a flap. On the outside the window is fitted with a copper grating to prevent the escape of radio-frequency power from the vessel during heating experiments. The grating reduces the scattered light intensity by about 25 %. A blackened tube surrounds the beam path between the window and the polychromators to absorb ambient light.

2.25 The Polychromators.

The 16 polychromators are installed in a cabinet shielded with Cu plating. Each polychromator can be tilted about a horizontal axis, laterally displaced and rotated about a vertical axis through its entrance aperture. The beam path in a polychromator is shown in Fig. 7.

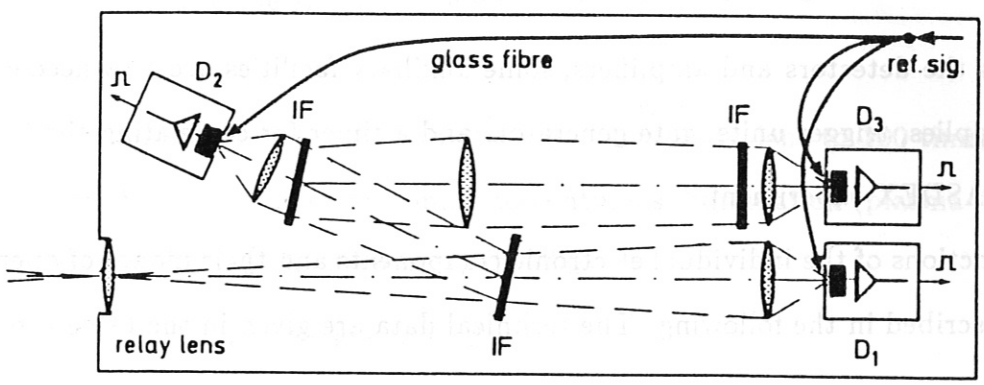

Fig.7: Diagram of a polychromator.

The field lens directly behind the $1 \times 7cm^2$ large entrance aperture images the large objective on the apertures of the detector lenses. The latter are combined with the avalanche diodes to form a unit which is rotatable about the vertical. The detector lenses, with a focal length of 50 mm and a clear diameter of 45 mm (f/1.2) have the purpose of imaging, reduced by 10 times, the entrance apertures ($1 \times 7cm^2$) of the polychromators on the avalanche diodes ($1 \times 7mm^2$ sensitive area). The first interference filter is incorporated in the beam path like a beam splitter so that the beam path to the second diode is optically equivalent to that of the first diode. After the second interference filter the cone of light expands and is additionally collimated by means of a viewing lens.

The collection optics transmits all the light incident on the large objective (f/5.5) from each 28 mm long scattering volume to the first two detectors. About 20 % of the light going to the third diode is lost.

2.3 Electronics.

The electronics for the multi-pulse scattering system in ASDEX have the following purposes:

- conversion of scattered light signals into electric signals;
- low-noise, broad-band amplification of signals to about 1 V;
- conversion of analogue signals to digital quantities.

Besides the detectors and amplifiers, some auxiliary facilities are also needed, such as power supplies, trigger units, gate generators and a timer for correlating the laser pulses with the ASDEX experiment.

The functions of the individual electronic components and their modes of operation are briefly described in the following. The technical data are given in the table (appendix).

2.31 Detectors (Avalanche Diodes)

Unlike photomultipliers, which are normally used in laser scattering, avalanche diodes are relatively unknown light detectors. Their advantages and disadvantages compared with multipliers are therefore described in detail in the following:

a) The quantum efficiency at 0.9 μm is max. 80 %. It decreases towards shorter and longer wavelenghts. At 1.064 μm it is still 45%.

b) The avalanche gain factor can assume values of up to 200.

c) The background noise of the diodes including the integrated amplifier is of the order $10^{-13}W/\sqrt{Hz}$. In the scattering experiment described it only dominates at plasma densities of $\leq 2 \times 10^{12} cm^{-3}$. At higher densities the noise of the measured light governs the measuring accuracy. This noise does not only depend on the number of charge carrier pairs measured but also on the gain factor of the diode (excess noise). The optimum operating point for the conditions in ASDEX is therefore at an avalanche gain factor of about 20.

d) Photosensitive area.

Avalanche diodes are available in various sizes. It should of course be noted that the frequency response, the homogenity of the amplification, and the signal to noise ratio decrease as the diode active area increases. The ordinary commercial version of the diodes used[1] has a diameter of 3 mm (surface area $7mm^2$) and frequency response to about 24 MHz. In ASDEX we use a special version of equal active area, but its dimensions of $1 \times 7mm^2$ are matched to the shape of the scattered volume.

e) Linearity.

The avalanche diodes are linear up to pulse intensities equivalent to 100 times that of scattered light in ASDEX. The same applies to continous illumination (plasma light). In this respect they are far superior to most multipliers.

f) Sensitivity to radiation and magnetic fields.

Apart from the usual precautions against electrical disturbances by copper shielding, no shielding from X-radiation, neutrons, or magnetic fields was provided in ASDEX. In fact, no spurious effects have been found. In this respect avalanche diodes are also superior to multipliers, particularly because of their small sensitive volume.

g) Temperature sensitivity.

The sensitivity of the diodes is temperature-dependent: a temperature rise by about 10°C reduces the sensitivity to approx. one half. To avoid heating of the diodes by the preamplifiers, the amplifiers are only powered during the ASDEX discharge. For long-time measurements (calibration in the laboratory) the momentary sensitivity has to be checked and be taken into account in the evaluation.

An unpleasant property of avalanche diodes was only noticed after lengthy operation: after illumination with intense continous light or after short-time overvoltage some diodes showed noise amplitudes up to ten times the normal values. With further operation, however, most of these diodes recovered in the course of a few days.

[1] Manufacturer: RCA; type: C-30950

2.32 Amplification of Signals.

The avalanche diode housing includes an integrated preamplifier (impedance transformer). An AC-coupled two-stage amplifier built at IPP amplifies the signals to the level necessary for the ADC's (approx. 1 Volt at 50 Ohm). The high frequency response of this amplifier (1 GHz), initially led to intrinsic oscillations as a result of feedback across signal and supply cables. Proper grounding of the avalanche diodes and other components eliminated this effect. Furthermore, heating of the avalanche diodes by the amplifiers was minimized by powering the amplifiers for just a few seconds during the plasma discharge. The avalanche voltage of approx. 400 Volts is continuously applied.

2.33 Choice of Frequency Response.

The avalanche diodes, including the integrated amplifier, have a maximum bandwidth of about 24 MHz. A low frequency limit for the two-stage auxiliary amplifier was set at about 340 Hz. The reason for this is that both the scattering signals with a duration of 30 ns and the 50μs wide square-wave signals (laboratory calibration) have to be transmitted. For measurements in ASDEX, a higher low frequency limit is preferred in order to reject fluctuations of the plasma light as good as possible. This is achieved by incorporating coupling capacitors of suitable capacitance in the measuring line (see Fig. A2 in the appendix).

When the low frequency limit is raised to about 16 kHz, the monitoring signal is reduced by about 4% of the preceding scattering signal due to undershooting. This effect is compensated numerically in the evaluation programme.

2.34 Pulse Transformer.

A fast pulse transformer with two galvanically decoupled outputs is connected in front of the input of the ADC's. It's functions are:

a) reverse the polarity of the signals;

b) transmit the scattering and monitoring signals galvanically decoupled to different ADC's;

c) reduce generally the negative offset voltage of the ADC inputs.

2.35 The Analog-Digital Converters (ADC's).

In ASDEX we use charge-sensitive ADC's of the type 2250L supplied by Le-Croy. These ADC's need at least 10 μsec for analogue to digital conversion. The 200 ns time interval between the signal and monitor therefore requires for separate ADC's for the scattering and monitoring. For this reason 96 ADC channels are used in ASDEX for 48 measuring channels.

The offset of the ADC's can be varied only within narrow limits and has to be preset to a positive value greater than the maximum negative amplitude of the noise.

The ADC's have a linear characteristic only at signal levels ≥ 2 counts; for small signal measurement it is therefore necessary (see 2.53, Raman calibration) to shift the operating point into the linear range by applying a DC voltage.

The upper limit of the digitalization range is 512 counts. The gain of the system has to be chosen accordingly. If signals exeed the dynamic range (e.g. with pellet injection), the gain can be reduced in a simple manner by lowering the voltage across the avalanche diodes by a few 10 V. The resulting reduced sensitivity of the diodes is automatically taken into account by the monitoring system in the evaluation procedure (see 2.61, Checking).

2.36 Triggering.

The reliability and accuracy of the entire scattering measurement depend to a large extent on exactly timed triggering of the ADC gates. The main trigger for the electronics is therefore provided by the laser pulses themselves: part of the laser light passed through the ASDEX vessel is transmitted to the shielded measuring cabinet by a lightguide of minimum length (9 m long), where it initiates the opening of the gates for the scattering signals by means of a fast Si-photodiode. In addition, the triggering electronics produces

the 200 ns delayed gates for the monitoring signals and the approx. 20 μs delayed gates for measuring the offsets.

To ensure a fixed delay between the scattering and monitoring gates, the delay is provided by a cable of definite length and transit time. It is also extremely important, especially in the case of small signal measurement (Raman calibration), that the gating time is constant within $\approx$1%.

2.37 The Clock.

To be able to compare the Thomson scattering measurements with time resolved recordings of other diagnostics, it is necessary to know the exact times of the laser pulses to establish correlations e.g. with pellet injection or sawteeth. For this purpose a quartz clock with a time resolution of 0.1 ms is started by the main trigger of ASDEX at the beginning of the plasma discharge and read out at every laser pulse by the data acquisition system.

2.38 Power Supply.

The avalanche diodes and the associated amplifiers are powered from the shielded cabinet in the control room via 20 m long cables. So far no disturbances of the electronic system by ASDEX during operation have been observed.

2.4 Data Acquisition.

As the ADC's cannot store all signals of the 400 laser pulses which are emitted during one discharge, the data have to be immediately transferred from the ADC's to a buffer memory (Le Croy 8801/16). This is done by a LSI-11 microprocessor. In addition to the measuring data, the processor also reads the quartz clock at every laser pulse. The datafile generated in the memory thus contains one time value and $3 \times 16 = 48$ scattering and monitoring signals and their offsets for each of the 400 laser pulses per discharge (= 193 signals/pulse). After the plasma discharge the data are transferred to the ASDEX computer.

2.5 Measuring Process.

The signals expected from the Thomson scattering have the following basic time behavior on each of the 48 channels (Fig. 8):

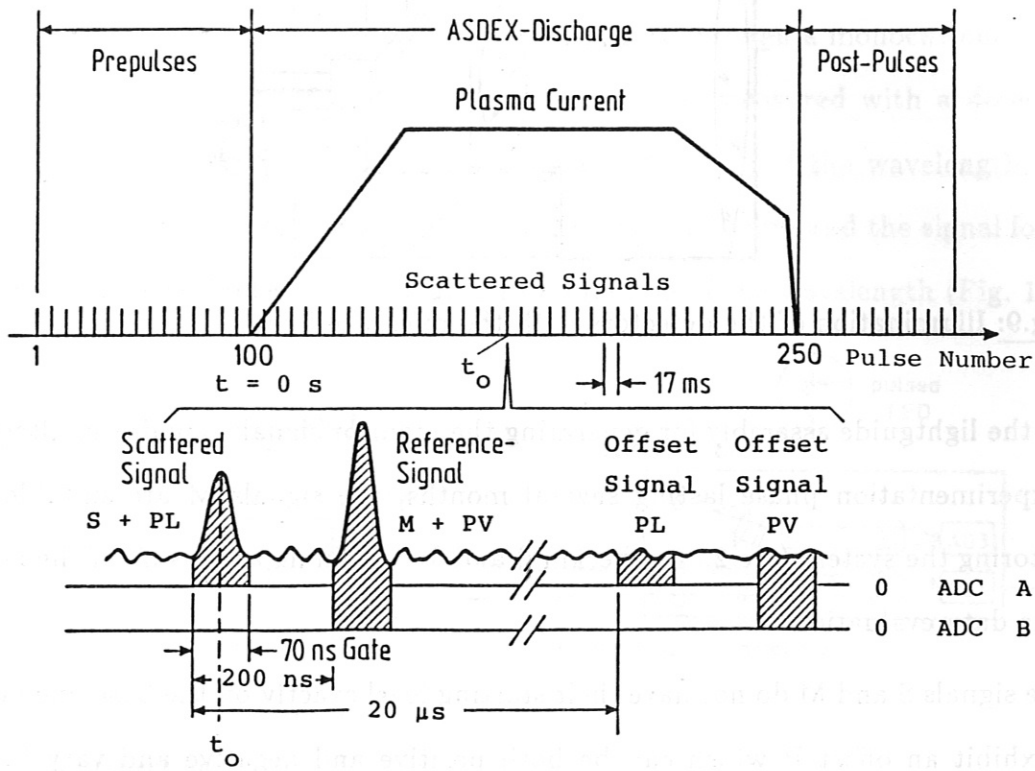

Fig.8: Sequence of the signals measured in an ASDEX discharge.

At time t_0, when the laser pulse passes through the plasma, the Thomson scattering signal S is observed. A reference signal M is generated by diffuse irradiation of each avalanche diode with the laser pulse which is delayed approx. 200 ns by a lightguide. After being delayed, the light for this signal is shared by the 16 polychromators through a 16-way lightguide fan and can be set to about the same intensity as by means of neutral density filters. The lightguide for each polychromator is, in turn, divided into three in order to illuminate the three spectral channels of each spectrometer simultaneously.

The individual diodes are illuminated by the bevelled ends of lightguides, as shown in Fig. 9:

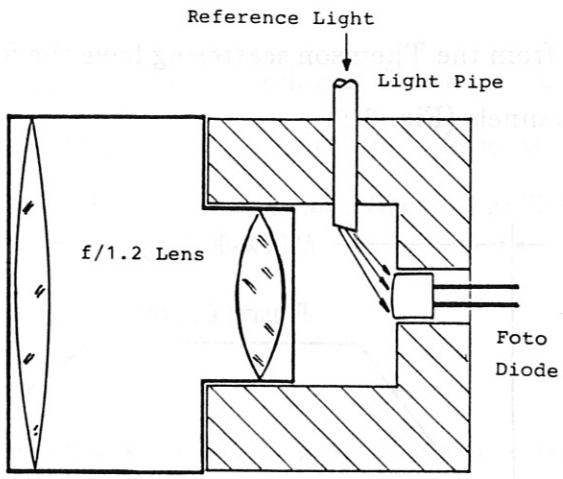

Fig.9: Illumination of the detectors with the reference light.

As the lightguide assembly for generating the monitor signals remains unaltered during an experimentation phase lasting several months, the signals M are suitable both for monitoring the system (see 2.61, Checking) and for attaining a measure of the laser power for the data evaluation.

The signals S and M do not have their starting level exactly on the base line (see Fig.8), but exhibit an offset P which can be both positive and negative and vary in the long term (e.g. within a few days). This offset is of electronic origin and has nothing to do with plasma light. The latter is equal to zero on average owing to the AC coupling of the amplifiers. The observable fluctuations of the offset signal are due to the fast fluctuations of the plasma light, the noise of the diodes, and the shot-noise.

The signals S and M and the offset P have to be recorded to evaluate the Thomson scattering signals.

For technical reasons the signals S and M can be separated not much more than about 200 ns from one another. Owing to the conversion time of the ADC's of about 10 μs, two separate convertors are needed to record the signals S and M. The above described electronic offset P is however different for each channel and therefore has to be measured separately as well (see Fig. 8, PL, PV).

2.51 Measurement of the Spectral Sensitivity of the Polychromators.

In order to evaluate the measured signals quantitatively, the spectral sensitivity of the 16 polychromators has to be attained in a preceding calibration measurement with relatively high wavelength resolution (approx. 10 – 20 measured points per filter). For this purpose the light of a stabilized tungsten ribbon lamp was passed through a monochromator with appropriate resolution. The intensity at the exit slit was measured with a detector of known spectral sensitivity (thermocouple array) as a function of the wavelength. Each individual polychromator was then illuminated with this radiation and the signal for each of the three avalanche diodes was measured as a function of the wavelength (Fig. 10).

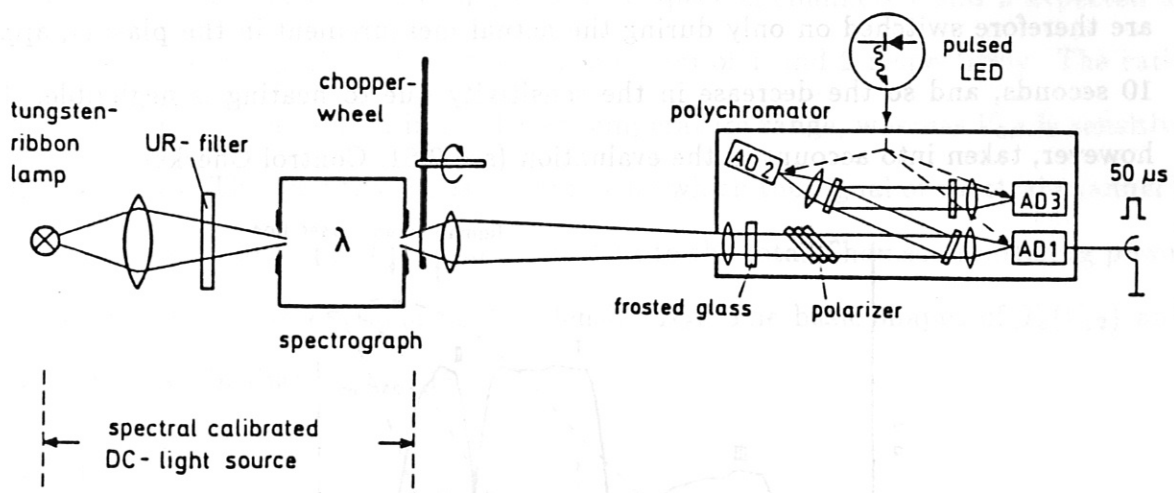

Fig.10: Laboratory setup for Te calibration of a polychromator.

In this measurement one has to pay attention to several important points:

- The light has to be chopped so that a signal can be observed at the output of the diode amplifier owing to the AC coupling. The measurements in our case were done with an almost rectangular pulse with a duration of about 50 μs which was produced by a chopper-wheel behind the exit slit of the monochromator.
- The light has to pass through the polychromator just as the Thomson scattering light. In particular, diode surfaces and interference filters have to be illuminated in the same way as during scattering on ASDEX. The reason for this is the possible variation of the diode sensitivity and filter transmission across area. Correct illumination of the

filters is particularly important for measuring the wings of the transmission curves if Raman calibration lines are expected in this region (see 2.53, Raman Calibration). As the aperture of the monochromator was not sufficient to illuminate the polychromator completely, a scatter plate was illuminated at its $1 \times 7\text{cm}^2$ entrance slit. The mounts of the succeeding filters and lenses guarantee the same illumination as during scattering on ASDEX.

- Any variation of the sensitivity of the avalanche diodes caused by temperature changes during the measurement has to be determined and taken into account in the calculation. In our case the heating of the amplifier end stage and hence of the diodes during the half-hour measuring time leads to a decrease in sensitivity of 5 – 10%. The amplifiers are therefore switched on only during the actual measurement in the plasma, approx. 10 seconds, and so the decrease in the sensitivity due to heating is negligible. It is, however, taken into account in the evaluation (see 2.61, Control Checks).

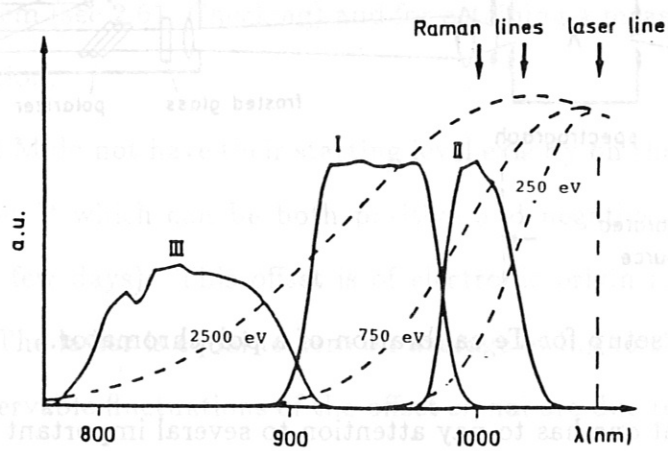

Fig.11: Spectral sensitivity of the three channels of a polychromator. This polychromator is one of the 12 polychromators which are equipped with relatively broad interference filters for measuring Te in the central plasma region.

2.52 Calculation of the Evaluation Functions for Te and Ne.

The spectral sensitivities $T_1(\lambda), T_2(\lambda)$ and $T_3(\lambda)$ of the three channels (see Fig. 11) of each polychromator, measured in the laboratory, were used to calculate numerically the following ratios as a function of the elctron temperature Te:

$$V_{12}(T_e) = \frac{\int \sigma(\lambda, T_e) T_1(\lambda) d\lambda}{\int \sigma(\lambda, T_e) T_2(\lambda) d\lambda} \tag{2}$$

and

$$V_{3S}(T_e) = \frac{\int \sigma(\lambda, T_e) T_3(\lambda) d\lambda}{\int \sigma(\lambda, T_e)(T_1(\lambda) + T_2(\lambda)) d\lambda} \tag{3}$$

and

$$V_N(T_e) = \frac{\int \sigma(\lambda, T_e) d\lambda}{\int \sigma(\lambda, T_e) T_2(\lambda) d\lambda} \tag{4}$$

where $\sigma(\lambda, T_e)$ is the scattering function of a plasma with Maxwellian velocity distribution of temperature Te (see 1.2, Physical Principles, eq. (1)).

$V_{12}(\mathrm{T}_e)$ is the ratio of the scattering signals of spectral channels 1 and 2 expected at temperature T_e, and $\mathrm{V}_{3S}(\mathrm{T}_e)$ the ratio of 3 and sum of 1 and 2 respectively. The ratio V_{12} is strongly dependent on T_e in the lower temperature range, whereas V_{3S} is sensitive to high T_e values. The quantity V_N is the factor by which the signal of spectral channel 2 has to be multiplied to obtain the value equivalent to the total Thomson scattering power and hence a quantity proportional to the density N_e. The basic shapes of $T_e(V_{12})$ and $V_N(T_e)$ are shown in Figs. 12 and 13:

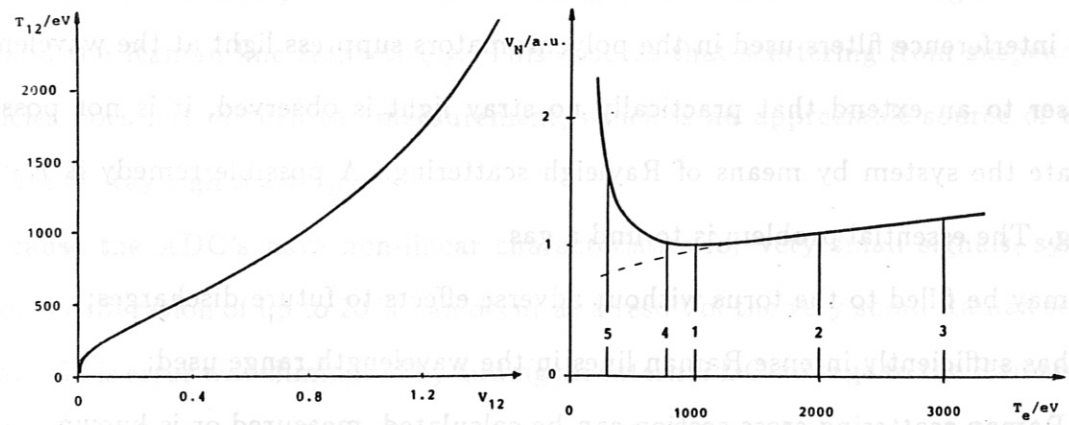

Fig.12 and 13: Plots of $T_e(V_{12})$ and $V_N(T_e)$.

Both functions were interpolated by analytical expressions:

$$T_e(V) \approx \underbrace{A + B\sqrt[3]{V}\, e^{CV}}_{I} + \underbrace{D(V-E)(V-F)(V-G)\, e^{HV^2}}_{II} \tag{5}$$

The parameters A, B, C in part I of eq. (5) are determined in a best fit programme. Addition of function II reduces deviations to $\leq 1\%$.

$$V_N(T_e) \approx U + \sqrt{V(T_e + W)} + Re^{-S\sqrt[3]{T_e}} \tag{6}$$

The quantities U, V, W in this case are calculated from three equidistant grid points (1, 2, 3 in Fig. 13) located right of the minimum of the function V_N, while R and S are determined from the remaining differences at the grid points in the minimum and on the left boundary (4, 5) of the temperature range.

These calculated quantities A to H for V_{12} and R to W for V_N are stored in the computer and linked to the evaluation programme; they remain valid until major changes to the system are made (e.g. realignment, replacement of filters, etc.). Any changes to diodes and amplifiers occurring in the course of the measuring period are detected by the monitor system after each discharge and taken into account quantitively (see 2.61, Control Checks). Repeated measurements have shown that the spectral sensitivity of the polychromators did not change within the error margins over more than a one years period.

2.53 Density Calibration by Means of Raman Scattering.

As the interference filters used in the polychromators suppress light at the wavelength of the laser to an extend that practically no stray light is observed, it is not possible to calibrate the system by means of Rayleigh scattering. A possible remedy is Raman scattering. The essential problem is to find a gas

- which may be filled to the torus without adverse effects to future discharges;
- which has sufficiently intense Raman lines in the wavelength range used;
- whose Raman scattering cross-section can be calculated, measured or is known.

All three requirements are satisfied by hydrogen (H_2). The scattering cross-section of the anti-Stokes rotational Raman lines was calculated and measured by us [**11**]. It is about 1/3000 of the Rayleigh scattering cross-section. Hydrogen of 80 mbar produces a Raman signal which is equivalent to the Thomson scattering signal of a plasma with

$7.2 \cdot 10^{10} cm^{-3}$ density. This value is only valid for the polarization component relevant to Thomson scattering. The magnitude of the Raman signals at ASDEX is of the same order as the detector noise. The signal to noise ratio can however be improved easily by averaging the 400 pulses of a pulse sequence. By doing this, the statistical error becomes smaller then 5% (Fig.14).

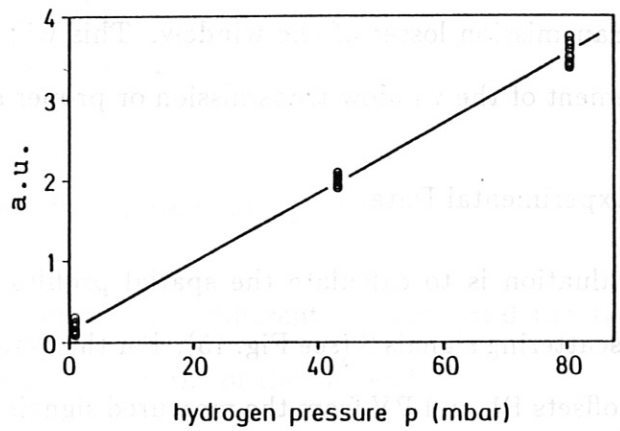

Fig.14: Calibration curve of one spectral channel. Each measured point is the average of the 400 pulses of a laser pulse sequence. About 60 pulse sequences are used for a Raman calibration.

A particular advantage of Raman scattering is the different wavelengths of the laser line and the Raman line respectively. This ensures that scattering from suspended dust particles does not disturb the measurement, which is an appreciable source of errors in the case of Rayleigh scattering.

Because the ADC's have non-linear characteristics for very small signals, systematic errors in calibration of up to 20 % can occur as a result of the very small Raman scattering signals. This error was eliminated by adding an external DC-voltage to the Raman signals, which was equivalent to about the amplitude of the Thomson scattering signal.

A second source of systematic error of similar magnitude occurs when one of the two roughly equal intense Raman lines coincides with the steep wing of an interference filter and when the transmission in the wing is not measured with sufficient accuracy (see 2.51, Measurement of the Spectral Sensitivity).

In the previous experimental period of about one year it was found that the density values measured by Thomson scattering immediately after Raman calibration agreed within ±10% with those obtained from the interferometer measurement. In the subsequent period the density values from Thomson scattering apparently became smaller and smaller than those from interferometry. The reason for this increasing discrepancy was accumulation of evaporated material on the observation window from the plasma side (wall material, carbon) which leads to transmission losses of the window. This will be remedied in the future by in-situ measurement of the window transmission or proper shielding.

2.6 Evaluation of the Experimental Data.

A first step of data evaluation is to calculate the spatial profiles of Te and Ne as a function of time from the scattering signals S (see Fig. 15). For this purpose, it is necessary to subtract the electronic offsets PL and PV from the measured signals. As the offsets may be assumed to be constant during a laser burst (typically 7 s), it is appropriate to form the average offsets for each channel and subtract these values. The averaged quantities $\overline{PL}$ and $\overline{PV}$ are therefore calculated separately for the two ADC's and subtracted from the measured quantities (S + PL) and (M + PV):

$$S \leftarrow (S + PL) - \overline{PL} \tag{7}$$

$$M \leftarrow (M + PV) - \overline{PV}$$

In this way the values S and M for every spectral channel (i), spatial channel (j) and laser pulse (n) are calculated (19200 numbers).

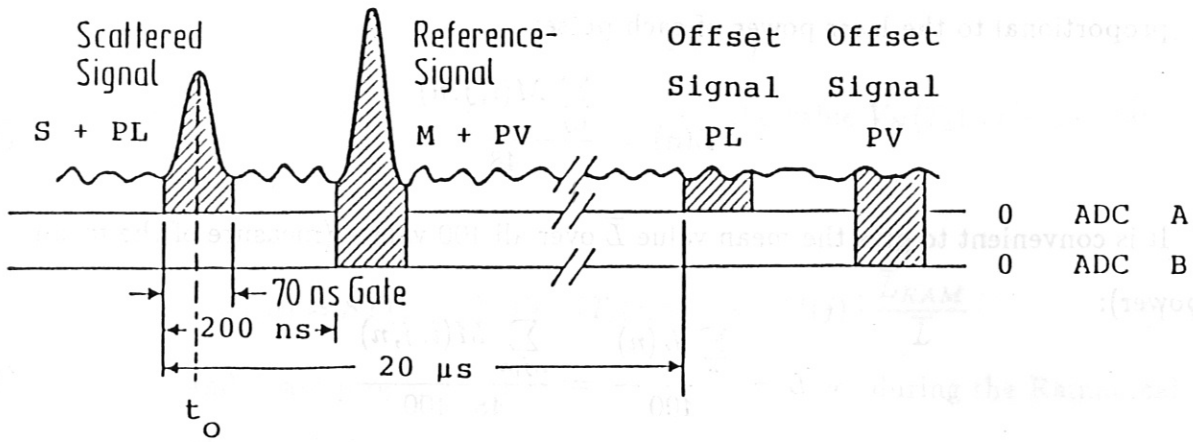

Fig.15: Evaluation of the measured signals.

The relative sensitivity of the different channels and the time evolution of the laser power can be calculated by means of the values M:

1. The value averaged in time over all n = 400 pulses of each channel is a measure of its sensitivity during the particular discharge. If the mean values of the i×j=48 channels are normalized to the sum of the mean values = 48, one obtains numbers E_{norm} of the order 1 which are independent of the laser power:

$$E_{norm}(i,j) = 48 \cdot \frac{\sum_n M(i,j,n)}{\sum_{i,j,n} M(i,j,n)} \tag{8}$$

Comparison with the corresponding values E_{null} of a reference discharge with known system sensitivity allows the deviation to be calculated:

$$E(i,j) = \frac{E_{norm}(i,j)}{E_{null}(i,j)} \tag{9}$$

and all scattering signals to be corrected:

$$S_{korr}(i,j,n) = \frac{S(i,j,n)}{E(i,j)} \tag{10}$$

The values of E are normally within 1.00 ± 5%.

2. The mean value L(n) of the monitor signals M over all i×j=48 spectral channels is proportional to the laser power of each pulse:

$$L(n) = \frac{\sum_{i,j} M(i,j,n)}{48} \tag{11}$$

It is convenient to give the mean value $\overline{L}$ over all 400 values (measure of the mean laser power):

$$\overline{L} = \frac{\sum_{n} L(n)}{400} = \frac{\sum_{i,j,n} M(i,j,n)}{48 \cdot 400} \tag{12}$$

and to normalize the individual values L(n) to the sum = 400 so that these values are also of the order 1:

$$L_{norm}(n) = \frac{L(n)}{\overline{L}} = \frac{\sum_{i,j} M(i,j,n)}{\sum_{i,j,n} M(i,j,n)} \cdot 400 \tag{13}$$

Divison by these values converts the scattering signals to the same laser power:

$$ST(i,j,n) = S_{korr}(i,j,n)/L_{norm}(n) \tag{14}$$

The next step is to establish whether there is stray light present and, if so, to subtract it from the scattered light. This is done by means of a group of 60 measured values S obtained before the ignition of the plasma discharge. The mean value from these pulses is then subtracted from each scattering signal. Experience with ASDEX shows that the stray light is negligible in relation to the Thomson scattered light. Only for the small signals of the Raman calibration has it to be taken into account.

To determine the temperature, one now has to form the ratios of the scattering signals of two spectral channels:

$$V_{12}(j,n) = \frac{ST(1,j,n)}{ST(2,j,n)} \tag{15}$$

The temperature is calculated with the approximation function (see 2.52, Evaluation of the data):

$$Te_{12}(j,n) \approx T_e(V_{12}(j,n)) \tag{16}$$

The density is derived from the signal ST (2, j, n), the value $V_N(T_e)$ and the Raman calibration value RAM(j):

$$N_e(j,n) \approx ST(2,j,n) \cdot V_N \cdot (T_e(j,n)) \cdot RAM(j) \cdot \frac{\overline{L}_{RAM}}{\overline{L}} \tag{17}$$

where $\overline{L}_{RAM}$ and $\overline{L}$ are proportional to the mean laser power during the Raman calibration and the plasma discharge, respectively.

It has hitherto been assumed that just one pair of signals ST (1, j, n) and ST (2, j, n) were measured per spatial channel. Since, however, each polychromator contains three diodes, there is another signal ST (3, j, n) available. This signal is used to form the ratio

$$V_{3S}(j,n) = \frac{ST(3,j,n)}{ST(1,j,n) + ST(2,j,n)} \tag{18}$$

which, however, only has reasonable values at high temperatures T_{e3S}.

The evaluation programme contains instructions whether a temperature is calculated from V_{12} or from V_{3S}, or whether a mean value is formed from the two temperatures. In an overlapping region in which both V_{12} and V_{3S} yield reasonable values, a weighted mean value of the temperatures is formed, where the weighting for Te_{3S} increases and that for Te_{12} decreases as the temperature increases. Superimposed on this weighting is an additional weighting factor which depends on the signal noise.

2.61 Checks, Safeguards, Records.

If all measured signals could be evaluated in a physically meaningful way, the evaluation method already discussed would be sufficient. Unfortunately, practice shows that there are also signals or combinations of signals which yield meaningless results if special checks are not built in and safeguards taken.

These signals include, in particular, measured values which are negative and signals whose ratios V_{12} or V_{3S} are beyond the range of validity of the approximation function

$T_e(V_{12})$ and $T_e(V_{3S})$ respectively. To avoid the termination of the evaluation when such cases occur, the relevant temperature and density values are replaced by special small numbers, which allow further calculation but, on the other hand, carry a code and reveal the type of error.

Moreover, it is appropriate to evaluate only those signals which are distinctly above the noise level. Signals below a given threshold are therefore treated likewise and lead to code numbers for Te and Ne as well.

If there are only occasional duds between signals otherwise easy to process, these are replaced by mean values formed from temperature and density values adjacent in time.

Before and after the plasma discharge the signals are within the noise level and should, of course, be not replaced by mean values of neighbouring measured points. The programme therefore contains the instruction to replace only up to four successive duds by mean values and, if there are more than four, to suppose that no plasma is present. In this case, Te and Ne are set equal to zero.

To track down errors in doubtful cases, it is, of course, possible to issue printouts which allow both the raw data and calculated values to be checked.

Records (Fig. 16) are routinely filed for every discharge. They allow assessment of the status of the entire Thomson scattering system within one discharge.

The title of the record includes: shot number, the value $\overline{L}$ as a measure for the mean laser power, the number of laser pulses occurred before the begin of the plasma discharge and the numbers of pulses used for calculation of the mean stray light $\overline{FL}$.

The following list contains the sensitivities E of all 48 channels in relation to the reference discharge, the normalized sensitivities E_{norm}, the mean values of the electronic offsets $\overline{PL}$ and $\overline{PV}$ and their mean noise amplitudes PLDEL and PVDEL. The mean stray light is named $\overline{FL}$. The column " MARK" assigns the crossing of given limits in the columns with corresponding numbers. The records also show the normalized laser power L_{norm} of every 7th laser pulse as a function of time.

SCHUSS 19973, $\bar{L}$: 125.2,PULSE VOR OH:115,FALSCHL.VON PULS: 1-115

Referenz-Schuß: 18812

J	I	E 1	E_{norm}	$\overline{PL}$	PLDEL 2	$\overline{PV}$	PVDEL 3	$\overline{FL}$ 4	MARK	L_{norm}	ZEIT
1	1	0.968	0.943	-7.92	0.69	-4.32	0.64	0.203	0	1.008	-1895.7
1	2	0.965	0.948	-7.84	0.55	-5.54	0.56	0.162	0	1.034	-1779.0
1	3	0.948	0.930	-7.89	0.56	-4.95	0.57	0.259	10000	0.974	-1662.3
2	1	1.017	1.130	-9.28	1.09	-7.05	1.23	0.318	0	1.088	-1545.6
2	2	1.013	1.283	-7.90	0.91	-7.77	1.00	0.029	0	1.074	-1428.9
2	3	1.025	1.107	-7.61	1.20	-5.88	1.15	-0.119	0	1.089	-1312.2
3	1	0.999	1.105	-8.03	1.13	-6.19	1.18	0.111	0	1.104	-1195.5
3	2	0.993	0.854	-6.56	0.85	-6.61	0.83	0.043	0	1.085	-1078.8
3	3	0.957	0.661	-8.88	0.80	-6.70	0.77	0.119	0	1.067	-962.2
4	1	1.008	1.648	-8.68	1.05	-6.20	1.13	0.055	0	1.093	-845.5
4	2	1.011	1.325	-8.10	1.00	-6.67	0.98	-0.039	0	1.027	-728.8
4	3	1.018	1.509	-8.52	1.11	-6.61	1.21	-0.026	0	1.016	-612.1
5	1	0.994	1.283	-5.63	1.00	-4.75	1.05	-0.352	0	1.055	-495.4
5	2	0.994	1.048	-6.94	0.83	-4.25	0.83	0.046	0	1.037	-378.7
5	3	0.991	1.355	-5.42	1.01	-4.86	1.18	-0.167	0	1.061	-262.0
6	1	1.045	1.525	-4.20	3.73	-2.83	4.53	0.497	2300	1.024	-145.3
6	2	1.036	1.581	-4.37	0.87	-4.02	0.90	-0.354	0	0.925	-28.6
6	3	1.038	1.528	-6.66	1.09	-3.77	1.04	0.106	0	0.938	89.4
7	1	0.933	0.448	-4.67	0.57	-3.32	0.64	0.132	10000	1.001	208.1
7	2	0.938	0.477	-5.08	0.49	-3.93	0.51	0.128	10000	1.058	326.7
7	3	0.941	0.464	-4.94	0.57	-3.93	0.64	0.169	10000	1.015	445.3
8	1	0.977	0.534	-6.49	0.66	-5.28	0.62	0.083	0	1.025	563.9
8	2	0.988	0.775	-5.80	0.77	-4.37	0.78	0.107	0	0.990	682.5
8	3	0.994	1.114	-6.27	1.13	-3.88	1.08	-0.044	0	0.959	801.1
9	1	1.000	1.129	-8.90	1.09	-6.44	1.05	0.088	0	0.919	919.7
9	2	0.996	1.027	-8.28	0.97	-6.75	0.89	0.170	0	0.970	1038.3
9	3	1.001	0.880	-6.98	0.98	-6.01	0.97	0.217	0	0.995	1157.0
10	1	0.974	0.947	-9.21	0.90	-6.59	0.89	0.158	0	0.972	1275.6
10	2	0.973	0.971	-7.72	0.77	-6.12	0.72	0.056	0	0.981	1394.2
10	3	0.977	1.043	-7.42	0.95	-6.85	0.91	0.146	0	0.983	1512.8
11	1	0.956	0.682	-6.81	0.96	-4.63	1.21	-0.001	0	0.954	1631.4
11	2	0.949	0.761	-6.12	0.61	-5.36	0.69	0.047	10000	0.917	1750.0
11	3	0.944	0.720	-5.74	0.65	-5.92	0.88	0.121	10000	0.977	1868.6
12	1	0.993	1.583	-5.14	0.98	-7.55	1.01	-0.136	0	0.903	1987.2
12	2	0.984	0.869	-6.02	0.94	-5.67	0.92	0.006	0	0.980	2105.8
12	3	0.979	0.967	-10.32	0.97	-6.48	0.99	0.161	0	0.995	2224.4
13	1	1.041	1.224	-6.40	0.90	-5.36	0.86	0.518	0	0.992	2343.1
13	2	0.995	0.939	-5.50	0.71	-5.57	0.68	0.201	0	1.031	2461.7
13	3	1.007	0.943	-5.91	0.94	-5.79	1.08	0.272	0	0.990	2580.3
14	1	0.977	0.590	-5.47	0.60	-3.97	0.59	0.224	0	1.004	2698.9
14	2	0.982	0.681	-5.07	0.52	-3.40	0.56	0.328	0	1.004	2817.5
14	3	0.967	0.551	-4.77	0.56	-2.88	0.49	0.286	0	0.964	2936.1
15	1	1.000	0.763	-5.82	0.88	-4.82	0.82	0.202	0	0.935	3054.7
15	2	1.002	0.587	-6.46	0.90	-5.23	0.84	0.471	0	0.968	3173.3
15	3	1.004	1.057	-6.07	1.08	-4.79	0.92	0.527	0	1.011	3291.9
16	1	1.036	0.863	-5.78	0.95	-4.94	0.91	0.257	0	0.955	3410.5
16	2	1.065	1.507	-5.00	2.39	-4.65	2.41	0.090	10000	0.973	3529.1
16	3	1.008	1.142	-5.68	1.63	-4.74	1.57	0.368	0	0.948	3647.8

Fig.16: Record for checking the performance of the system.

In addition, about two test shots are recorded every experimental day to check whether any signal- and monitor line has changed. The usual records cannot provide this information because the sensitivities recorded are only calculated from the monitors and do not use the signal lines. In a test shot, light signals from a system of 16 light-emitting

diodes are shone on all 48 detectors, and recorded simultaneously. The light pulses have a duration of about 500 ns and are timed such, that the S and M channels are irradiated with the same amount of light during the opening times of the two ADC's. If the system works properly, the signals S must yield the same relative sensitivities of the 48 channels as the signals M.

2.62 Calculation of the Temperature and Density Profiles.

Because of the ASDEX geometry, the measurement of the Thomson scattering light is done along a vertical cord which is displaced with respect to the centre of the vessel by 1.75 cm towards the torus axis. One thus obtains temperature and density profiles as a function of the coordinate z along this cord ($-40cm \leq z \leq 20cm$).

Assuming the plasma pressure, the temperature and density on a flux surface are to be constant, it is physically meaningful to plot these values not as a function of the coordinate z, but as a function of the flux surface radius ρ. For this purpose the coordinates z of the scattering volumes have to be expressed as a function of the flux surface radii ρ on which they are located.

In a tokamak these flux surfaces, however, depend in a complicated way on the plasma pressure and magnetic field.

The shift due to the plasma pressure can be divided into a displacement of the "outermost" flux surface ($\rho = a$) and a superposed shift Δ of the embedded flux surfaces. It is assumed that the circular cross-section is conserved. The radial shift of a flux surface is a function of its minor radius ρ; its maximum value is attained at $\rho = 0$, the magnetic axis. It can be approximated by:

$$\Delta(\rho, t) \approx \Delta_0(t)(1 - \frac{\rho^2}{a^2}) \tag{19}$$

where $\Delta_0(t)$ is the time-dependent shift of the magnetic axis. This can be represented as a linear function of $\beta_p + l_i/2$. Equilibrium calculations [**12**] yield:

$$\Delta_0(t)\,[m] = -0.019 + 0.045(\beta_p + l_i/2) \tag{20}$$

(β_p = mean plasma pressure/poloidal field pressure at the plasma boundary (r = a), ℓ_i = normalized internal inductance).

The general case of an ASDEX flux surface configuration is shown in Fig. 17:

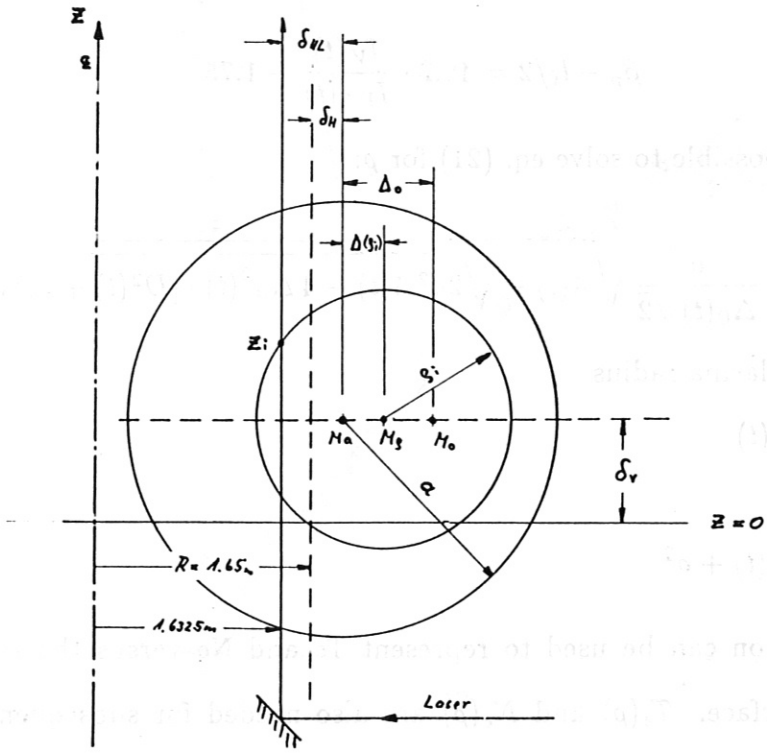

Fig.17: Flux surface configuration in ASDEX.

The centre of the outermost flux surface with radius $\rho = a$ is generally shifted with respect to the geometric centre of the vacuum vessel (R=1.65 m, z=0), both vertically and horizontally. The scattering volumes are located on the cord at R=1.6325 m and at the fixed heights $z_1, z_2 \ldots z_{16}$.

From figure 17 the following geometric relation can be deduced:

$$\rho^2 = [\Delta(\rho,t) + \delta_{HL}(t)]^2 + [z - \delta_V(t)]^2 \tag{21}$$

with

$$\delta_{HL}(t) = \delta_H(t) + 1.75\,cm \tag{22}$$

δ_H and δ_V are the horizontal and vertical shifts of the plasma column which are measured by magnetic induction probes. $\Delta(\rho,t)$ is calculated from eqs. (19) and (20).

$(\beta_p + l_i/2)$ can be derived from the current I_V through the vertical field coil, which is feedback-controlled in ASDEX to keep the plasma in its radial position, and from the plasma current I_{PL}. For ASDEX the relation

$$\beta_p + l_i/2 = 48.2 \cdot \frac{I_V(t)}{I_{PL}(t)} - 1.75 \tag{23}$$

holds. It is now possible to solve eq. (21) for ρ:

$$\rho(z,t) = \frac{a}{\Delta_0(t)\sqrt{2}} \sqrt{A(t) - \sqrt{2a^2 A(t) - 4\,{\Delta_0}^2(t) \cdot [D^2(t) + {z_1}^2(t)]}} \tag{24}$$

with a = minor plasma radius

$D(t) = \delta_{HL} + \Delta_0(t)$

$z_1(t) = z - \delta_{v(t)}$

$A(t) = 2D(t) \cdot \Delta_0(t) + a^2$

This transformation can be used to represent Te and Ne versus the radius ρ of the appropriate flux surface. $T_e(\rho)$ and $N_e(\rho)$ are also needed for subsequent calculations (eg. energy content).

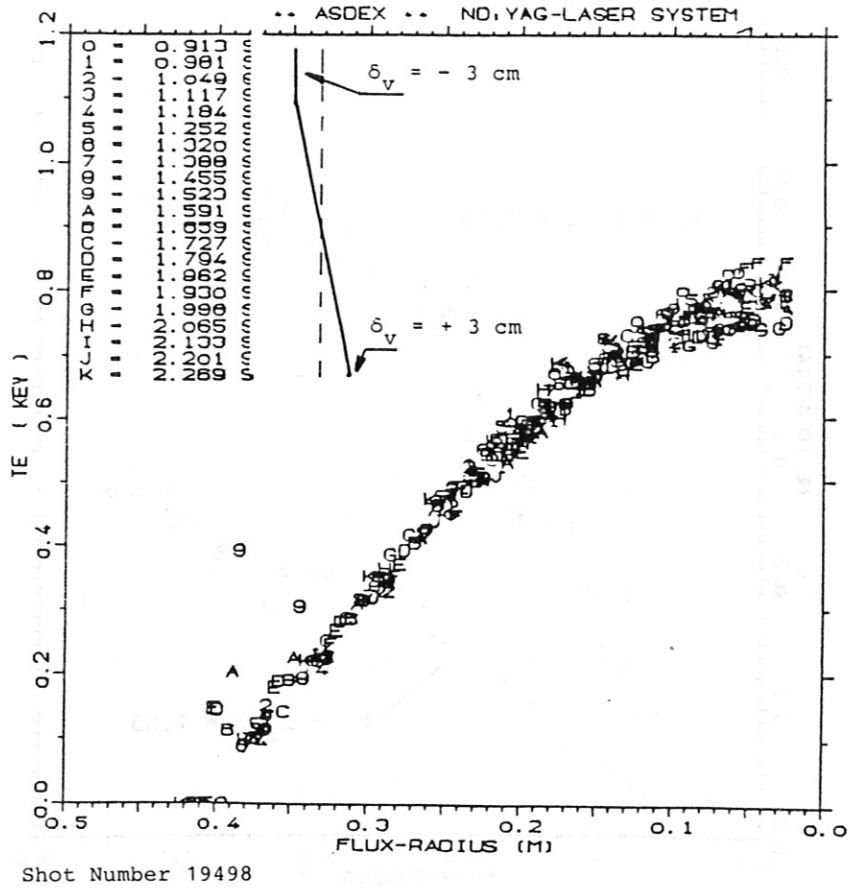

Fig.18: Profiles calculated as a function of the flux coordinate during a vertical displacement of the plasma column.

Figure 18 shows as an example 21 profiles $Te(\rho)$ of a discharge in which the plasma was vertically shifted from $\delta_v = -3cm$ to $\delta_v = +3cm$ without changing other plasma parameters.

Consequently Te(ρ) remains unchanged after the transformation (eq. 24).

Figure 19 shows the density profile of a discharge with additional heating. Owing to the rise of the β_p value the plasma centre is shifted outwards relatively to the outer flux surface; the result is an outward movement of the magnetic axis and its displacement of more than 10 cm from the laser beam at maximum heating.

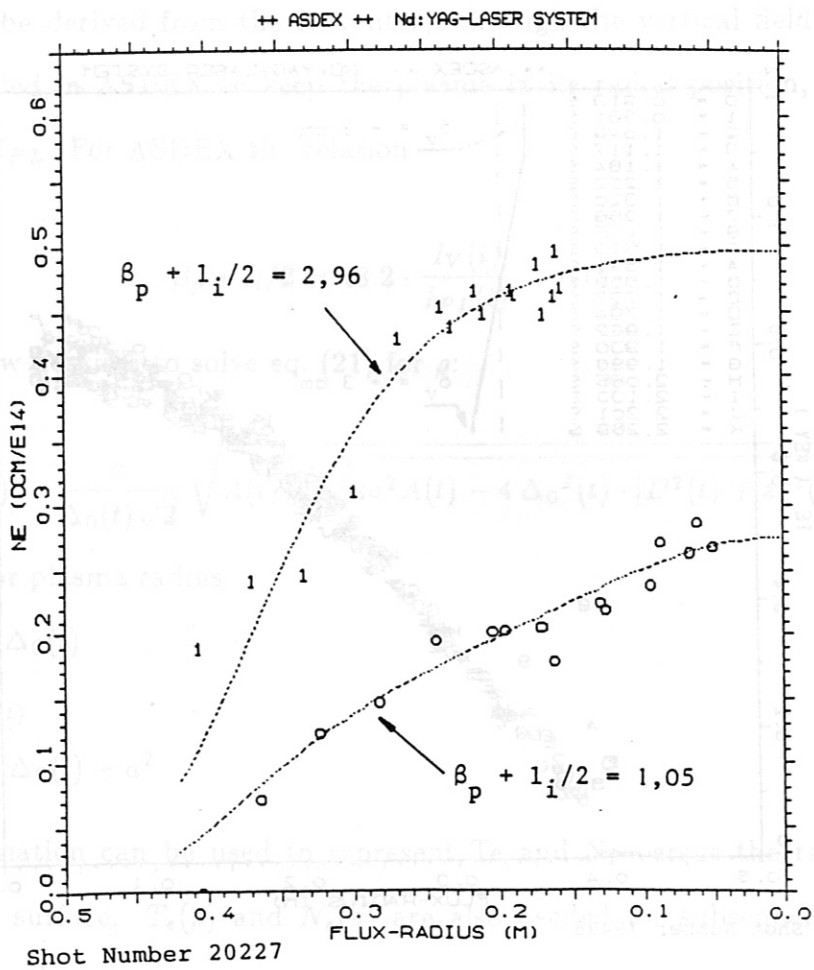

Fig.19: Density profiles for different values of β_{pol}.

Calculatons of additional plasma parameters often need measured Te/Ne-profiles. For this purpose, it is practical to approximate the shape of the profiles measured by Thomson scattering by an analytic expression.

The exponential function

$$f(\rho) = exp(a_0 + a_2\rho^2 + a_4\rho^4 + a_6\rho^6) \tag{25}$$

has proved to be suitable for representing all profiles measured in ASDEX so far. It is used in the standard evaluations. Besides the measured values, Fig. 19 shows the profiles adapted by means of the function in eq. (25). The coefficients a_i for $Te(\rho)$ and $Ne(\rho)$ for every laser pulse are automatically stored in a data file. They can be used for deriving integral quantities and functions of $Te(\rho)$ and $Ne(\rho)$.

It is of course appropriate to perform radial integrations in the coordinate system, which is matched to the flux surfaces. For this purpose the torus is divided into N = 100 flux tubes whose centres are located in accordance with eq. (24) and whose major and minor radii are $R_0 + \Delta(\rho_i)$ and ρ_i (i = 1....N). Thus, the volume element between two successive flux surfaces with the radii ρ_i and ρ_{i+1} is:

$$\Delta V_i = 2\pi^2[\, R_0(\rho_{i+1}^2 - \rho_i^2) + \Delta(\rho_{i+1}) \cdot \rho_{i+1}^2 - \Delta(\rho i) \cdot \rho_i^2] \tag{26}$$

with

$$R_0 = 1.65\, m + \delta_H$$

This simplification allows volume integrals to be replaced by sums. The expressions for the temperatures and the densities averaged over the volume are:

$$\ll T_e \gg = \frac{1}{\pi a^2} \int_0^\infty T_e(\rho) 2\pi\rho d\rho \approx \frac{1}{V_0} \sum_i T_e(\rho_i) \Delta V_i \tag{27}$$

$$\ll N_e \gg = \frac{1}{\pi a^2} \int_0^\infty N_e(\rho) 2\pi\rho d\rho \approx \frac{1}{V_0} \sum_i N_e(\rho_i) \Delta V_i \tag{28}$$

with $V_0 = 2\pi^2 a^2 R_0$ as torus volume.

Similarly, the density averaged over the line of sight can be calculated for arbitrary radii to allow direct comparison with the HCN interferometer measurement (see Fig. 20):

$$\overline{N_e}(s) = \int_0^\infty N_e(r_{eff}) db = \sum_{i=1}^{N} N_e(r_{eff}) \cdot \Delta b \tag{29}$$

$$r_{eff} = \sqrt{s^2 + b_i^2}\,; \quad \Delta b = \frac{1.2 \cdot a}{100}\,; \quad b_i = i \cdot \Delta b$$

For $b_i \geq 1.2 \cdot a$ it's assumed that $N_e = 0$.

The radial shift of the flux surfaces does not play any role in this calculation.

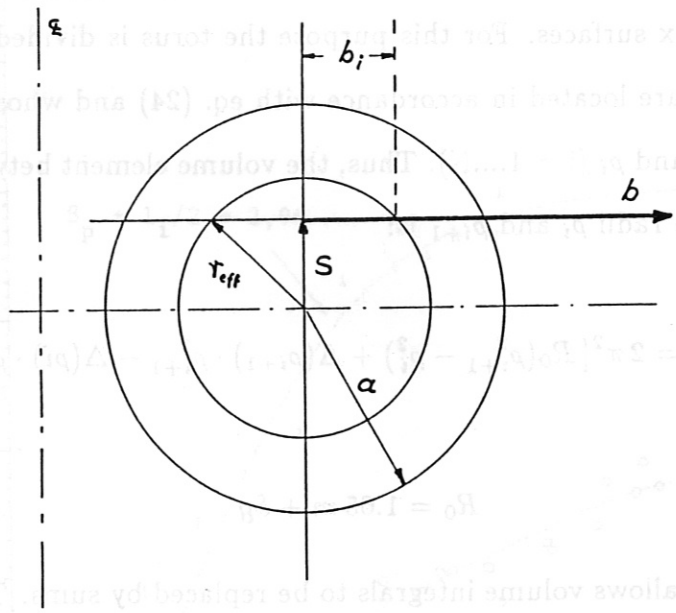

Fig.20: Geometry for calculating the integrated density along a line of sight.

Finally, the total thermal energy of the elctrons and its component β_{pe} of the total β_p are calculated:

$$E_e = \int_V 3/2\ N_e\, kT_e\, dV\ = 2.4\ J \sum_{i=1}^{N} \frac{N_e(\rho_i)}{[10^{20} m^{-3}]} \cdot \frac{kT_e(\rho_i)}{[eV]} \cdot \frac{dV_i}{[m^3]} \tag{30}$$

and

$$\beta_{Pe} = \frac{\ll P_e \gg}{\frac{1}{2}\mu_0 H^2} = \frac{2}{3}\,\frac{E_e}{V_0}\,\frac{(2\pi a)^2}{\frac{1}{2}\mu_0 {I_{PL}}^2} = 1.29 \cdot\ 10^9 \frac{E_e[A^2]}{{I_{PL}}^2[kJ]} \tag{31}$$

Figure 21 shows the time development of some parameters calculated with the results of the Thomson scattering:

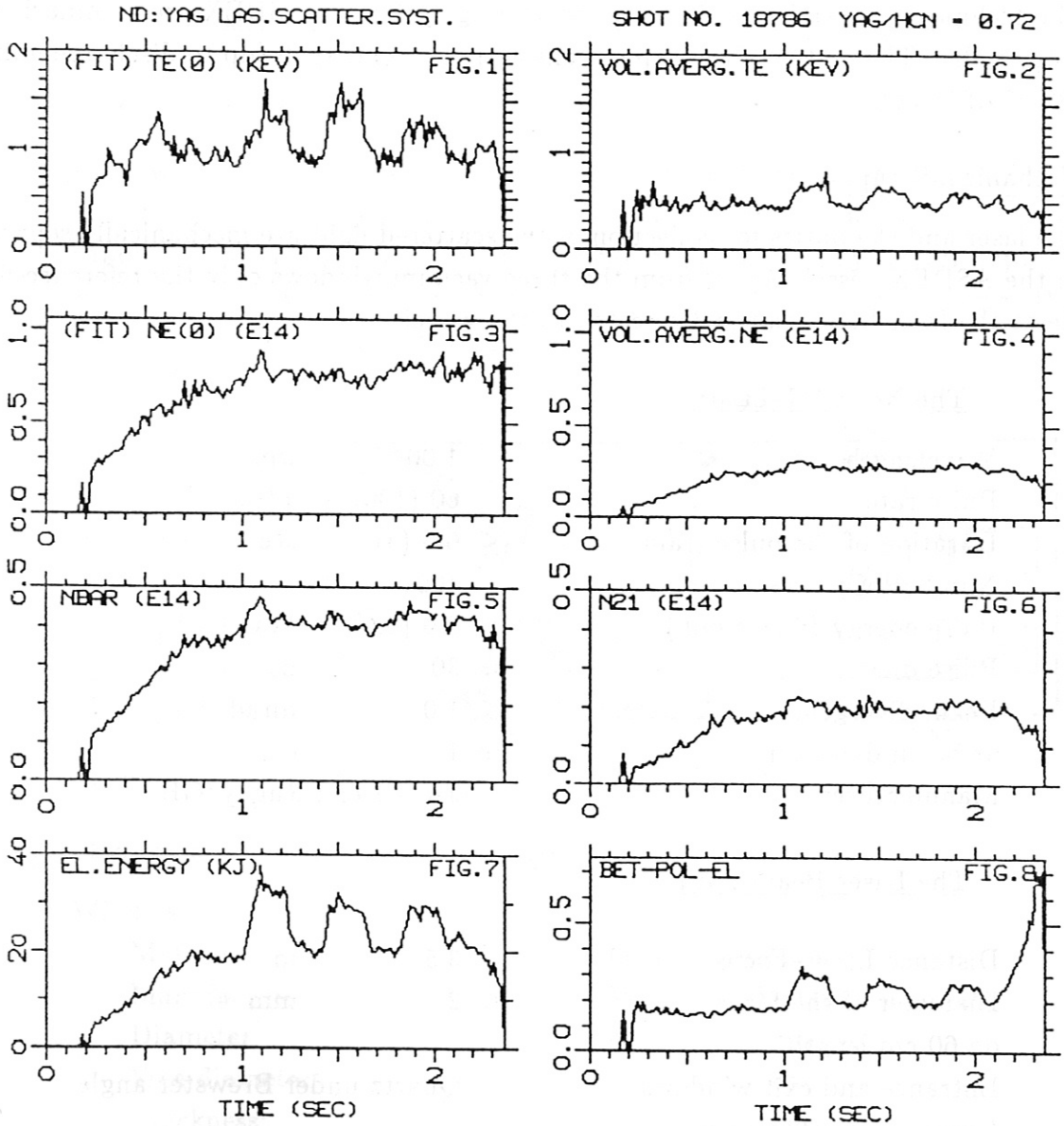

Fig.21: Plasma parameters derived from the results of the laser scattering:

TE(0) and NE(0) are the values on the magnetic axis extrapolated by equation (25). VOL.AVERG.TE and VOL.AVERG.NE are averaged over the volume of ASDEX. NBAR and N21 are density integrals along a central line of sight at z=0 and z=21 cm. EL.ENERGY is the total energy of the elctrons; BET.POL.EL is the poloidal beta of the elctrons.

3. APPENDIX.

The technical properties of the Laser scattering system at ASDEX are summarized in this appendix. The status of the experiment is that of mid 1986 (up to discharge number 20282 of ASDEX).

Mechanical Setup.

The laser and the optics for collection of the scattered light are mechanically separated from the ASDEX-vessel. Apart from the three vacuum windows only the reference-light-guide at the laser beam exit is connected to the vessel.

The Nd–YAG–Laser.

Wavelength		1.064	μm
Pulse rate		60 (100)	$1/sec$
Duration of the pulse train	$\leq$	6.6 (4)	sec
Number of pulses		400	
Pulse energy (linear pol.)	$\approx$	0.9 (0.6)	Ws
Pulse duration	$\approx$	30	ns
Beam divergence	$\leq$	1.0	mrad
at beam diameter	$\approx$	1	cm
Manufacturer		JK–Lasers; Rugby/GB	

The Laser Beam Path.

Distance Laser–Focus		3.5	m
Diameter of the focus	$\leq$	2	mm
on 60 cm length			
Entrance and exit windows		Quartz under Brewster angle	
Laser beam attenuation			
to about 1% :		Green glass plates, 10 cm thick under Brewster angle	

Light guides.

Reference light guide:			
Diameter of the bundle:		2	mm
Diameter of fibres:		50	μm
Length:		40	m

Light guide in order to trigger the datamation system:

Length:	9	m
Additional data	the same as reference guide	

Beam path of the scattered light.

A simple viewing dump is installed in the ASDEX vacuum vessel at the inner wall. It is composed of tilted and blackened steel plates. The vacuum window can be protected against evaporation at the plasma side during cleaning discharges by a steel flap. A Cu-grid at the outside of the window prevents the exit of high frequency power (Lower-Hybrid wave at about 1 GHz) out of the ASDEX vessel.

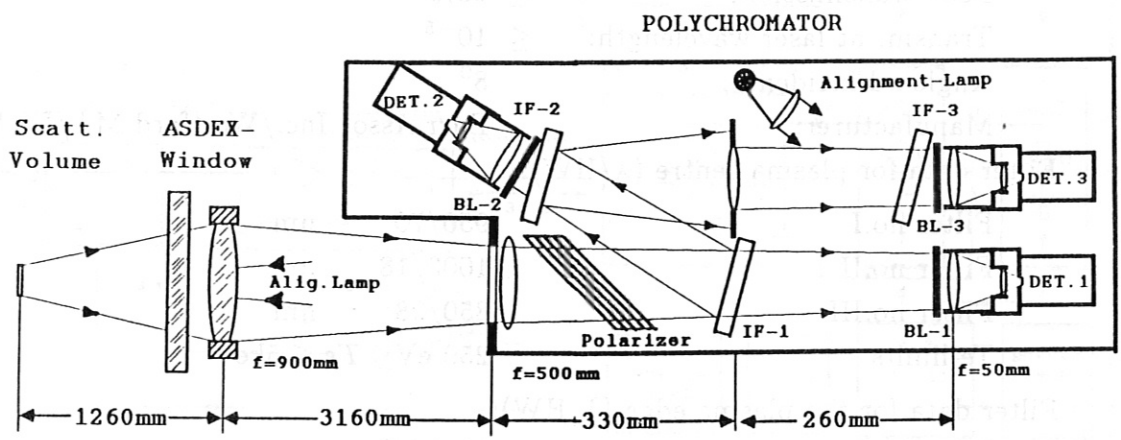

Fig.A1: Beam path of scattered light including polychromator.

Window:

Material:	Quartz type 124	
Manufacturer	Westdeutsche Quarzschmelze	
Diameter	46	cm
Free diameter	40	cm
Thickness:	4	cm
Width of the Cu-grid:	1	cm
Transmission of the Cu-grid:	74%	

Light dump:

Thickness of the plates:	0.5	mm
Distance between plates:	12	mm

Large objektive:

The large objective for imaging the scattering volumes was developed especially for this purpose; it was calculated for a very small curvature of the image plane. The lenses are anti-reflection coated.

Free diameter:	23	cm
Focal length:	90	cm

Number of lenses:	4
Manufacturer:	Ludwig Wolf/Neukirchen

Polychromators.

The 16 polychromator boxes are equipped with different sets of 3 interference-filters: 12 sets have relatively broad transmission in order to measure Te in the centre of the plasma; 4 polychromators have narrower filters matched to low temperature at the plasma edge. The blocking at the blue side of the spectrum is done by separate blocking filters.

Data of the filters:

Diameter:	6	cm
Peak transmission:	$\geq$ 80%	
Transm. at laser wavelength:	$\leq 10^{-5}$	
Angle od incidence:	8^0	
Manufacturer:	Barr.Assoc.Inc./Westford MA/USA	

Filter data for plasma centre (λ/HW):

Filter no.I	950/70	nm
Filter no.II	1003/18	nm
Filter no.III	850/98	nm
Te-limits	250 eV$\leq Te \leq$ 5keV	

Filter data for the plasma edge (λ/HW):

Filter no.I	1000/42	nm
Filter no.II	1030/21	nm
Filter no.III	940/61	nm
Te-limits	125 eV$\leq Te \leq$ 2.5keV	

Field lense in the polychromator:

Focal length	500	mm
Diameter	75	mm

Detector objektives:

Manufacturer	Isco/Göttingen	
Type	Kiptaron	
Focal length	50	mm
Cone	f/1.2	

Viewing lense:

Focal length	200	mm
Diameter	60	mm

All single lenses are made of BK7-glass.

Electronics.

For detection of the scattered light 48 Si-avalanche-diodes with integrated amplifier (hybrid-amplifier) are used. These diodes are especially manufactured with respect to the shape of their light sensitive areas. All other specifications correspond to the type RCA/C-30950.

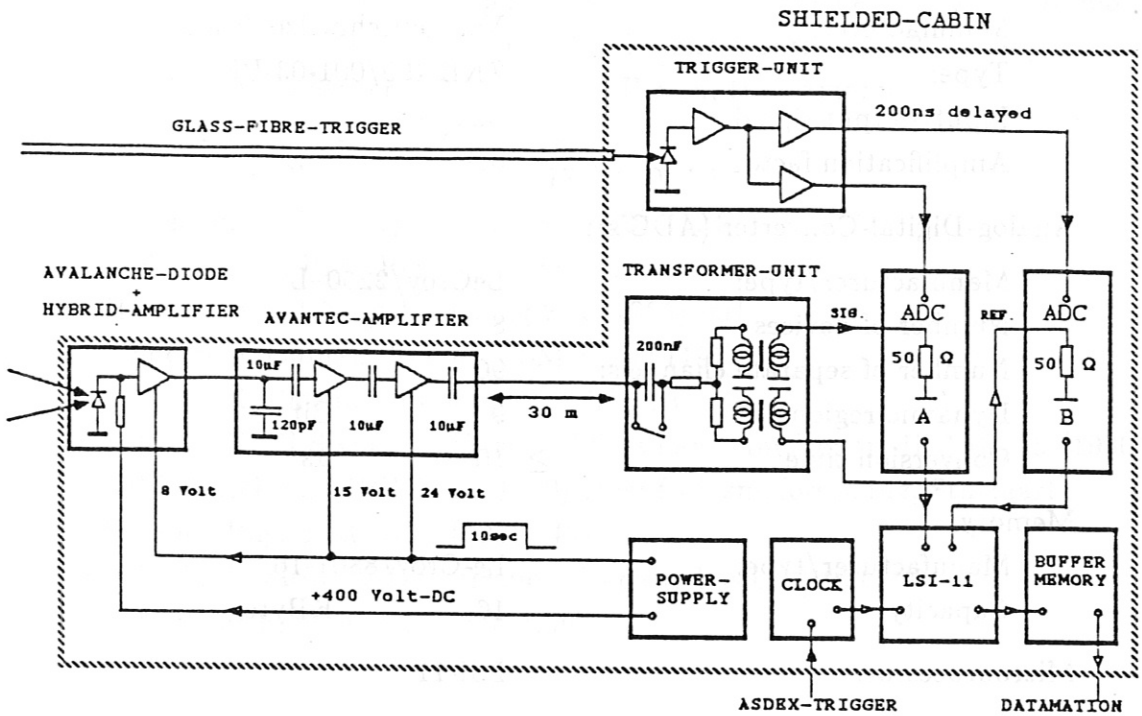

Fig.A2: Schematic of the electronic part of the scattering device.

Detectors:

Manufacturer/type	RCA/C 30950	
Sensitive area	$1 \cdot 7$	mm^2
Bandwidth	$\leq$ 24	MHz
Amplific.by aval.eff. (max.)	$\geq$ 20 (200)	
Equiv. noise power (NEP)	$1.6*10^{-13}$	$W/\sqrt{Hz}$
Max. quantum efficiency	0.8	at 0.9 μm

Avantec amplifier:

IC-types/manufacturer	GPD-462/463/Avantec	
Number of stages	2	
Voltage amplification factor	25	
Maximum exit voltage	1.5	V
Bandwidth	340 Hz–26 MHz	

Transformer unit:

The 48 transformer units enclose 2 pulse transformers each. The lower frequency limit of the system can be decreased by switching off a capacitor of 200 nF.

Bandwidth at calibrations:		$2.5 \cdot 10^3 - 5 \cdot 10^7$	Hz
Bandwidth at measurements:		$16 \cdot 10^3 - 5 \cdot 10^7$	Hz
Pulse transformer:			
Manufacturer:		Vacuumschmelze/Hanau	
Type:		ZKB 409/001-03-PF	
Input/output signal		pos./neg.	
Amplification factor		0.5	
Analog-Digital-Converter (ADC's):			
Manufacturer/type:		LeCroy/2250–L	
Number of devices		8	
Number of separate channels:		96	
Dynamic region		9	Bit
Conversion time	$\geq$	10	μs
Memory:			
Manufacturer/type:		Le-Croy/8801-16	
Capacity:		16	KByte
Microprocessor:		LSI-11	
Pin-diode in the trigger unit:			
Manufacturer/type:		Siemens/SFH-202	

REFERENCES:

/1/ E.Fünfer,B.Kronast,H.J.Kunze Phys.Letts.,Vol.5 (1963) 125

/2/ M.J.Forrest et.al. Culham Report CLM–R 107 (1970)
N.J.Peacock et.al. Nature 224 (1969) 488

/3/ R.Behn Phys.Lett. 74A (1979) 316
R.Behn, H.Röhr, K.-H.Steuer, D.Meisel, Appl.Phys.Lett. 36 (1980) 363

/4/ H.Murmann, M.Huang, Plasma Physics and Contr. Fus. 27 (1985) 103

/5/ H.Röhr, K.-H.Steuer,G.Schramm, K.Hirsch, H.Salzmann
Nuclear Fusion, 22 (1982) 1099-1102

/6/ J.Lasalle, P.Platz, Opt.Comm. 17 (1979) 325
J.Lasalle, P.Platz, Appl.Opt. 18 (1979) 4124

/7/ E.E.Salpeter, Phys.Rev. 120 (1960) 1528

/8/ H.J.Kunze, Z.f.Naturforschung 20a (1965) 801

/9/ J.Sheffield, Culham Report CLM-P 292 (1971)
J.Sheffield, Plasma Physics 14 (1972) 783

/10/ H.Röhr, K.–H.Steuer, K.Hirsch, H.Salzmann, Int.Report IPP III/55 (1980)
(IPP–Garching), IPF 80–2 (1980) (Inst.f.Plasmaforschung, Stuttgart)

/11/ H.Röhr, Phys.Lett. 81A (1981) 451

/12/ V.S.Mukhovatov, V.D.Shafranov, Nuclear Fusion (1971) 605

/13/ K.Lackner private communication.

We wish to express our thanks to

Dr.K.Hirsch and Dr.H.Salzmann of the " Institut für Plasmaforschung" of the University of Stuttgart, whose investigations in the forefield played an essential role for the successful installation of the new scattering system at ASDEX;

Mr. H.Czich and Mr. G.Schramm for their work on the electronics of the exeriment;

Mr. K.Förster and Mr. H.Strobl for their help at the technical setup of the scattering device; Mrs. D.Pohl and Mrs. T.Wendt for their help in developing the evaluation programmes.